DETERMINATION OF THE MINIMUM IGNITION ENERGY (MIE) OF PREMIXED PROPANE/AIR

By

My Ngo

A thesis submitted in partial fulfilment of the requirements for the Master of Science Program in Process Safety Technology

Department of Physics and Technology
University of Bergen, Norway
June 2009

TABLE OF CONTENTS

ABSTRACT

This Master thesis describes an experimental study aimed at determining the minimum ignition energy (MIE) of premixed propane/air mixtures. Two fundamentally different circuits have been employed for creating the sparks in the experiments: a replica of the American Society for Testing and Materials (ASTM) apparatus (ASTM, 2007) and an improved version of the synchronized spark generator described by Randeberg *et al.* (2006).

The explosion vessel was a 0.20 dm^3 cylindrical plastic tube, equipped with two 1.6 mm flat-ended tungsten electrodes. In the present work, the electrodes were flanged with glass plates and the spark gap was set to 2.0 mm.

The principle of the capacitive spark circuit of ASTM was to charge an appropriate capacitance connected across the spark gap through a large resistor (10^{12} Ω) by a high-voltage power supply until the spark occurred. Different spark energies could be obtained mainly by varying the value of the capacitance.

Premixed propane/air was used as test gas. About 220 tests were performed with the ASTM circuit to find the boundary between ignition and no-ignition in propane/air mixtures. The investigated propane concentrations were in the range 3.5 to 8.0 vol. %. By following the approach of Moorhouse *et al.* (1974), the MIE in the present work was determined by drawing the highest possible boundary line through all the experimental points that had no ignition points below it. This resulted in a minimum ignition energy of 0.48 mJ at a propane concentration of 5.2 vol. %. This is twice the value reported by Lewis and von Elbe (1961), but in very good agreement with the result obtained by Moorhouse *et al*..

The quenching effect of the 2.0 mm spark gap for propane/air mixtures of less than 4.0 vol. % was confirmed. However, the present results do not indicate that 2.0 mm is the quenching distance for any specific concentration on the fuel rich side in the investigated concentration range (3.5-8.0 vol. %). According to the data reported by Lewis and von Elbe, a flanged spark gap of 2.0 mm should correspond to the quenching distance for a propane/air concentration of about 6.0 vol. % on the fuel rich side.

The probability of ignition for propane/air mixtures of 5.2 and 5.5 vol. % were also studied by varying the spark energy levels in the range 0.40 to 0.75 mJ for both concentrations. Based on the classical U-shaped curve by Lewis and von Elbe (1961), presenting MIE as function of propane concentration, it was expected that a mixture of 5.2 vol. % propane in air would be more ignitable than a mixture of 5.5 vol. %. However, the present results do not show any significant difference in the ignitability for the two concentrations. By applying a statistical model to the data at each of the two concentrations, MIE for 1% probability of ignition were calculated. They were both significantly higher than the Lewis and von Elbe value of 0.25 mJ.

Randeberg *et al.* (2006) described a spark generator for producing synchronized capacitive spark discharges of low energy, down to below 0.1 mJ. However, Eckhoff *et al.* (2008) re-examined the discharge circuit of Randeberg *et al.*, and concluded that, due to the hidden subtle energy supply, the real spark energies in the experiments were significantly larger than those quoted in the published paper. The additional energy in the discharge was of the order of 1 mJ.

With the aim to minimize the additional energy, an improved version of the Randeberg *et al.* (2006) spark generator was constructed, which reduced the additional energy input to the order of 0.25 mJ.

However, this required a considerable effort and time. Hence, due to lack of time, the experimental work for the determination of MIE as a function of propane/air concentration was not completed. Therefore, it was decided to perform a series of tests at one propane concentration only. The propane concentration of 5.2 vol. % was selected, because this was the concentration given the lowest ignition energy in the ASTM spark generator tests. About 50 tests were performed to determine the highest total spark energy below which there were no ignitions. A firm conclusion cannot be drawn due to the limited number of tests. However, the experimental data indicate a MIE value for 5.2 vol. % propane/air mixtures of 0.36 mJ, which is lower then the MIE value obtained by using the ASTM method (0.48 mJ).

It was observed that the shape and amplitude of the tail/undershoot of the spark pulses varied from test to test, indicating that the synchronized-spark generator requires further improvement.

ACKNOWLEDGEMENTS

This study was conducted at the Department of Physics and Technology, University of Bergen, Norway. As in many other experimental studies, the process of building and commissioning the test system was quite a challenge and proved to be more time consuming than expected. Personally I found the last year of the Master's program to be tough, but also educative.

First of all I would like to thank my supervisor, Professor Rolf K. Eckhoff for his invaluable guidance, understanding and support. His devotion for knowledge has been truly inspiring. My special thanks goes also to senior engineer, Werner Olsen, my second supervisor, without whom it would not have been possible to construct the new spark generator. Through the past year I have learned a lot from him.

It has been a hard year, and I would like to thank my family and friends for their love and support. My classmates have been helpful throughout the project. I will also thank Martin Hansen from the Department of Chemistry, Professor Ivar Heuch from the Department of Mathematics, and senior engineer Kåre Slettebakken and his staff in the Mechanical Workshop at the Department of Physics and Technology for their contributions.

I would like to thank Trygve Skjold of GexCon AS for lending me some of the reading materials. Last but not least I wish to express my gratitude to the ELSTATIK foundation in Germany for sponsoring this project and associate Professor Bjørn J. Arntzen for his tips and advices throughout the project.

CHAPTER 1: INTRODUCTION

1.1 GENERAL OVERVIEW

1.1.1 Background

A key concern in process safety is to prevent explosions and mitigate their effects. Over the years, safety technology in the industry has improved continuously. These days, most industries in "the industrialized world" are operating on a reasonably high safety level. Although explosions in the process industries still happen. The concerns nowadays are not just on human life and material losses, but also on the potential impact on the environment. Therefore, process safety continuous to be important in the industry throughout the world.

An *explosion* is often identified by a loud noise, or "bang" resulting from the sudden release of energy. A more precise definition in the present context (Eckhoff, 2005) is to define an explosion as an exothermal chemical process that, when occurring at constant volume, gives rise to a sudden and significant pressure rise. Accidental explosions in the process industries include gas, spray/mist and dust explosions. These three categories of chemical explosions have similar ignition and combustion properties.

In the oil and gas industries, most gas explosions happen when combustible gas from accidental releases, mixes with air in the atmosphere and generates an explosive cloud. If the fuel/air ratio in the cloud is within the flammability limits, and there is a presence of an ignition source, an explosion will occur.

1.1.2 Ignition sources

Explosive gas mixtures can be ignited by many types of *ignition sources* or sources of energy that initiates combustion (Babrauskas, 2003). (Eckhoff, 2005) lists the following 8 types of ignition sources:

- open flames
- glowing or smouldering materials
- hot solid surfaces
- burning metal particles and "thermite" flashes from impacts, grinding, etc
- electrical and electrostatic sparks, arcs, and other forms of discharges

- jets of hot combustion gases
- adiabatic compression
- light radiation

Extensive reviews of the standard test methods and published experimental studies concerning the determination of critical ignition parameters, such as T_{min} (minimum ignition temperature) and MIE (minimum ignition energy), for gaseous fuel-air mixtures can be found in the books of Babrauskas (2003) and Magison (1998). These parameters can vary substantially with the actual ignition source characteristics, the dynamics, pressure and temperature of the gas mixture.

1.1.3 Minimum ignition energy concept

The term minimum ignition energy (MIE) is an important parameter in explosion hazard evaluation. It refers to the smallest amount of energy that an electric spark discharge must have to cause an ignition of a given gas mixture at given conditions.

For the last century, many experimental studies have been done to investigate the true values of the minimum ignition energy for different hydrocarbon fuels. MIE values depend not only on the composition of the mixture, but also on the method of the spark generation and properties of the electric circuit. Parameters such as gas concentration, pressure, temperature, flow characteristics, spark gap length, and discharge duration also influence the MIE.

1.1.4 MIE theories

There are two basic theories of ignition process by electric sparks: The *electrical model* considers transport of chemical energy by the internal diffusion of reactants and reaction products while *the thermal model* considers the transport of the thermal energy i.e. heat. Even while no complete ignition theory was available, Strid (1973) concluded that the hypothesis of thermal ignition seemed to be supported by the experimental MIE determination. A recent overview of ignition theories is given by Babrauskas (2003).

According to the *thermal theory* of electric spark ignition of Lewis and von Elbe (1961), the spark establishes instantly a small volume of hot gas immediately after the discharge. At first the temperature within this flame kernel increases rapidly, but as the ignition volume grows in size, the temperature decreases due to the flow of heat to the ambient unburned gas. In the adjacent layer of ambient gas the temperature rises and induces chemical reactions, so that a combustion wave is formed and propagates outwards. At the time that the temperature within the flame kernel has decreased to the order of normal flame temperature, the diameter of the flame kernel must have grown to a certain size for self-sustained combustion, i.e. ignition, to be established. The flame kernel has more or less a spherical shape. If the size is too small, the heat loss to the

unburned gas continuously exceeds the heat gain by chemical reaction, so that the reaction will gradually cease, leading to the extinction of the combustion wave (after only a small amount of gas around the original spark has burned). The minimum ignition energy is the energy required to establish the flame kernel of the minimum critical size for subsequent self-sustained flame propagation. Figure 1.1 gives an overview of the energy balance for electric spark discharge based on the thermal theory.

The *electrical theory* of electrical spark ignition supposes that the electrical discharge activates the chemical reaction by producing free radicals/ions in the discharge zone, which diffuse into the surrounding gas and initiate a self-propagating combustion chain. Therefore the ignition conditions of the mixture are dependent on the concentration of the reactive particles.

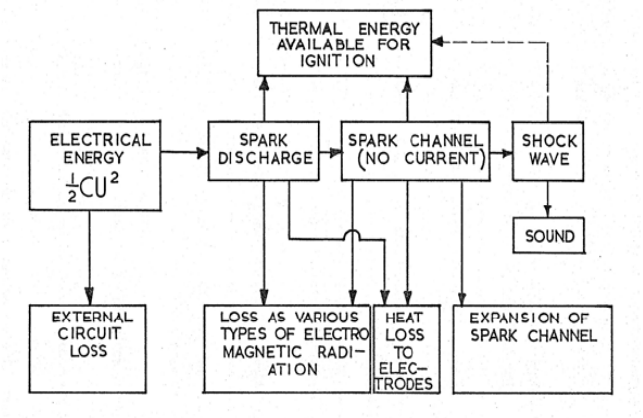

Figure 1.1*: Energy balance of an electric spark discharge based on the heat (thermal) theory. From Eckhoff (1970).*

In practice, accidental electrical spark discharges are usually of capacitive nature i.e. electrostatic discharges. Babrauskas (2003) divides discharges which have caused accidental ignitions into 6 different categories; *corona, brush, powder heap, spark, propagating brush* and *lightning-like discharge*. In the present work, only spark discharges are used as ignition source. Appendix A.1 provides more detailed definitions of these terms.

1.1.5 MIE in relation to incendivity of electrostatic discharges

The commonly published minimum ignition energies for most alkanes in air at normal temperature and pressure are of the order of 0.25 mJ. According to Lüttgens and Glor (1989), corona discharges have an equivalent energy of less than 0.02 mJ. This indicates that corona discharges may only be effective ignition sources for the easiest ignitable gases like hydrogen, acetylene and CS_2. However, according to Babrauskas (2003), in reality, it is unlikely that a corona discharge will ignite flammable atmospheres at all due to its diffuse nature.

Brush discharges on the other hand can generate equivalent spark energies of up to 3 mJ, and the very energetic propagating brush discharges can generate up to 10^5 mJ. Hence, these two discharge types are effective ignition sources for most explosive gas mixtures. Crowl (2003) emphasised that it is also important to remember that the MIE of 0.25 mJ is a very low energy, e.g. corresponding to the kinetic energy of a small coin as it impacts a surface after being dropped from a height of only a few millimetres. An electrostatic discharge that can be felt by a person has an energy of at least 20 mJ, i.e. about two orders of magnitude greater than 0.25 mJ. Therefore, the elimination of ignition sources should not be relied on as the sole defence against fires and explosions of gases and vapours.

1.1.6 Spark discharge features that may influence spark incendivity

The establishment of a self-sustained flame front in the combustible gas mixture is strongly influenced by the discharge mode and the geometry of the plasma volume, generated by the spark discharge. The total energy involved plays only a minor role. Maly and Vogel (1978) divided the spark discharge process in three main phases: *breakdown, arc* and *glow* phases. Any spark ignition system includes a different combination of these three discharge modes, with varying energy content and durations depending on the discharge circuit. Figure 1.2 shows both gap voltage and current vary as functions of time during a spark discharge.

With a very short spark durations of the order of 10^{-9} s (1 ns) more than 80% of the energy is transformed into plasma during the breakdown phase. The arc and glow phases last much longer and their energy transfer efficiencies are much less. A more detailed description of the characteristics of the three discharge phases are given in Appendix A.2.

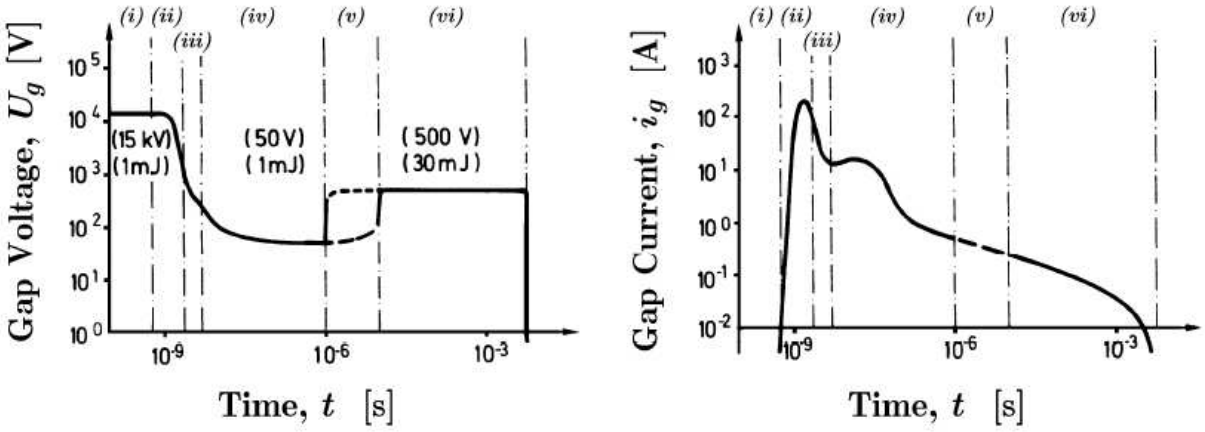

Figure1.2*: Schematic diagram of voltage and current vs. time in a spark discharge of a typical spark ignition system. The six discharge phases are: i) pre-discharge, ii) breakdown, iii) breakdown/arc transition, iv) arc, v) arc/glow transition, and vi) glow. From Maly and Vogel (1978)*

1.1.7 “Break” sparks and “jump” sparks

It is useful to distinguish between two types of electric sparks, viz. *break spark* and *jump spark*.

Break sparks occur when a circuit carrying an electric current is broken. The character of the break spark depends on the relationship between the inductance and the ohmic resistance in the circuit. The spark energy can usually be calculated by the formula $E = ½ Li^2$, where L is the inductance and i the current.

Jump sparks are caused by the release of electrical energy stored on a capacitor across a spark gap. The spark energy is calculated by the formula $E = ½ CU^2$ where C is the capacitance and U is the voltage. The capacitor energy is in electrostatic form and the spark occurs when the voltage of the spark gap reaches the breakdown voltage.

1.2 OBJECTIVE OF THE PRESENT WORK

The work described in this thesis consists of two main phases:

Phase 1

a) Construction of a copy of the ASTM standard apparatus (E 582 - 07) for determination of MIE for explosive premixed gases.
b) Determination of MIE for propane/air as a function of vol. % propane in the mixture, using the standard ASTM apparatus.
c) Analysis of results by comparing with available published data.

Phase 2

a) Construction of an improved version of the new electric spark generator for producing synchronized capacitive spark discharges of low energies, as indicated by Eckhoff *et al.* (2008). The aim of the improvement is to minimize the additional energy contribution to the effective spark energy due to the minute stray current following the main current pulse from the discharge capacitor.
b) Determination of MIE for propane/air as a function of vol. % propane in the mixture, using the new, improved synchronized-spark generator.
c) Comparison of results from 1b)/c) and 2b).

CHAPTER 2: REVIEW OF PREVIOUS WORKS

2.1 MIE AND QUENCHING DISTANCE

The quenching distance, QD**,** is the smallest distance between two surfaces that permits laminar flame propagation in a homogeneous quiescent explosive gas mixture to take place in the space between them. In relation to electric spark ignition, the term quenching distance refers mostly to the minimum distance between the electrodes which allows optimal ignition, with a minimal energy loss to the electrodes.

The QD is a very important parameter for MIE determination. It does not only depend on the composition of the gas mixtures, but also the pressure. Figure 2.1 shows MIE and QD increase when pressure and oxygen fraction in the gas mixture decrease. For any given combustible gas in air, the minimum spark energy for ignition and the QD vary with the concentration of the combustible gas in the mixture. For a given set of test conditions (temperature and pressure), the absolute MIE is found when the gas mixture is of its optimum/most ignitable concentration. QD also increases with increasing flow velocity, but decreases when the initial temperature of the mixture is increased. According to Lewis and von Elbe (1961), quenching distance of propane/air mixture of near 5.0 vol. % at 1 atm was around 1.8 mm.

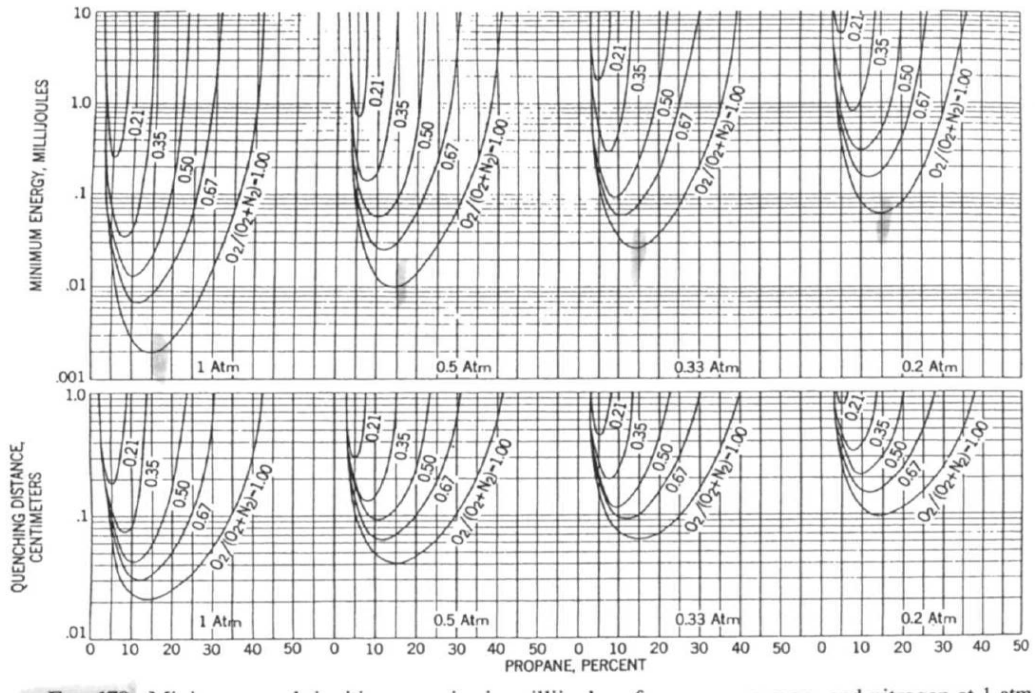

Figure 2.1*: Minimum energies of propane/oxygen/nitrogen at pressure range of 0.2 to 1 atm, and the quenching distances between flanged electrodes for the same mixtures. From Lewis and von Elbe (1961).*

As pointed out by Babrauskas (2003), the most effective spark gap length for ignition is slightly greater than the QD. If the electrodes are placed closer together than the QD, they will act as a heat sink and remove heat from the developing flame kernel, and therefore the required ignition energy will increase. Figure 2.2 indicates that the size and shape of electrodes do not significantly affect the values of MIE at electrode distances larger than the QD. But for smaller distances, the influence of these factors are significant. Flanged electrode is an extreme situation as indicated by the sharp and quite dramatic increase of MIE as soon as the spark gap becomes less than the QD. This is due to the cooling effect of the flanges, which prevents a laminar gas flame from propagating outwards from the spark between the flanges.

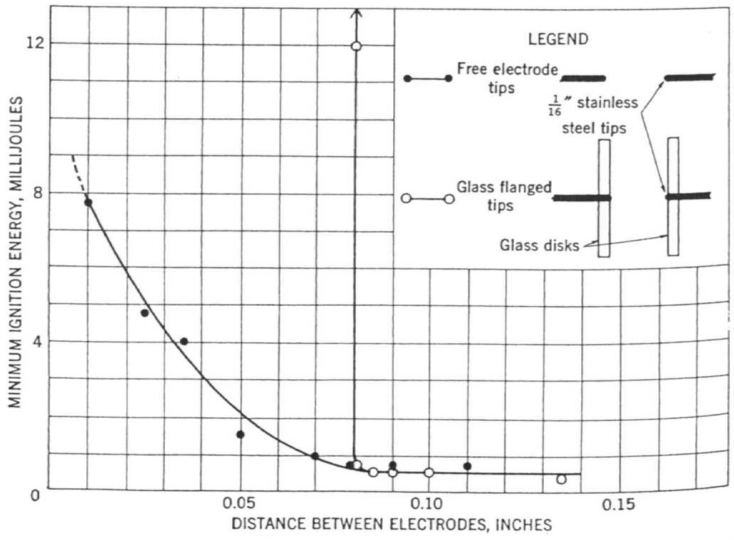

Figure 2.2*: Minimum ignition energies for free and glass-flanged electrode tips as a function of electrode distance. Stoichiometric mixture of natural gas (about 83% CH4 + 17% C2H6) and air at 1 atm pressure was used. From Lewis and von Elbe (1961)*

As mentioned earlier, the minimum spark energy for ignition is a function of the gas concentration of the mixture. Figure 2.3 shows the minimum ignition energies for different hydrocarbon fuels as U-shaped functions of the gas concentration. The minimum ignition energy, MIE, is defined as the minimum value of the U-shaped function.

It should be noticed that the fuel-air equivalence ratio Φ at which the MIE occurs increases with increasing carbon number, exhibited a steady shift toward fuel rich conditions. Due to the higher diffusivities, MIE of molecules lighter than air (for example like hydrogen and methane) occurs in lean mixture, i.e. when the fuel equivalence ratio, $\Phi < 1$. Figure 2.3 shows MIE value of methane is slightly higher than those of the higher alkanes.

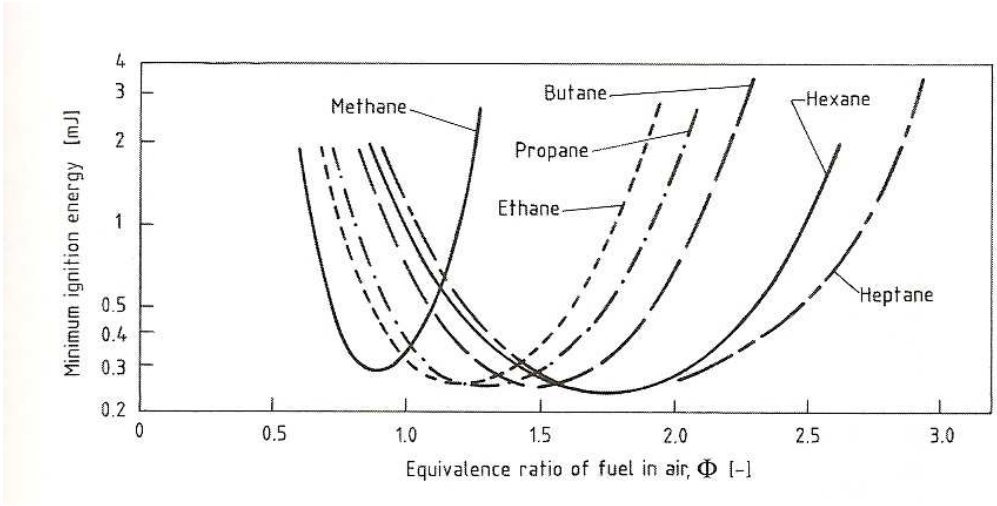

***Figure 2.3**: Minimum capacitive ignition energies of various gaseous alkanes/air mixtures as a function of the volumetric ratio of fuel and air. From Eckhoff (2005)*

Besides their studies of the influence on MIE of pressure and composition of the mixture, Lewis and von Elbe (1961) also studied the relationship between the quenching distance and MIE, by using glass flanged electrodes. Figure 2.4 shows that there is quite strong correlation between MIE and QD. The lower the MIE is, the shorter is the QD. The relation between MIE and QD can be reviewed in published literature. Most theories indicate the MIE values for gas/air mixtures are equivalent to the power 3 of QD. However, the experimental data collected by Lewis and von Elbe seemed to be proportional with the power 2 of the QD.

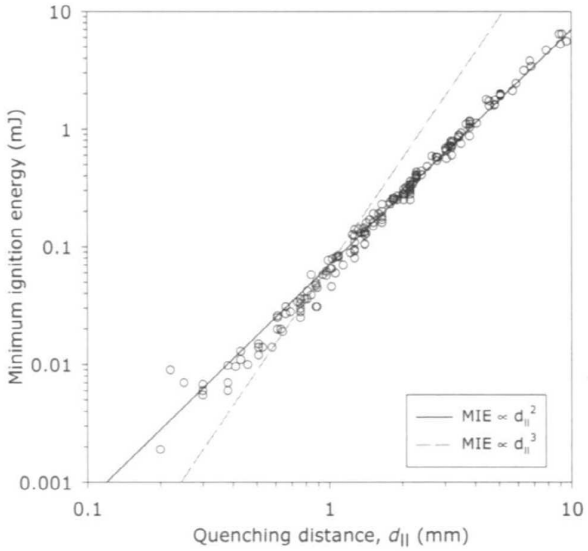

***Figure 2.4**: The relation between the quenching distance and MIE based on data with flanged electrodes (data for hydrogen, methane, ethane, and propane are included, but there is no effect of fuel type on relation). From Babrauskas (2003).*

2.2 THE STUDY OF LEWIS AND VON ELBE

2.2.1 Overview

The classical MIE data reported by Lewis and von Elbe (1961) are often referred to as absolute standards. According to the results of their experimental work, MIE of propane/air mixture was 0.26 mJ at ambient conditions. The optimal concentration for ignition was about 5.3 % vol.

2.2.2 Test apparatus

The original apparatus was first described by Guest (1944) and later modified by Blanc, Guest, von Elbe and Lewis (1947). The stainless steel test bomb had an inner diameter of 127 mm and the spark gap was located in the centre. The gap length could be adjusted by a built-in micrometer. 1.6 mm diameter pointed and flanged electrodes were used to determine MIE for different conditions. Glass flanges were mostly used because metal flanges are electrically conductive and had a tendency to cause ignition even within the quenching distance.

However, due to the electrical conductivity of the glass surface, Lewis and von Elbe did observe irregular discharges, particularly corona discharges, during their experiments even with glass flanges. To eliminate this source of error, the glass flanges could be coated with paraffin wax. But according to Strid (1973), Litchfield (1967) pointed out that the flanges should in fact be slightly conductive in order to equalize the electric potential.

2.2.3 Electrical spark-generation circuits

According to Kravchenko (1984), the spark generated by the circuit of Lewis and von Elbe had durations down to 1μs, indicating that their spark discharges were arc discharges. All tests conditions were controlled to eliminate energy losses. The energy storage capacitance could be varied over the wide range from 1 pF to 5000 pF, using two different apparatuses.

Electric circuit for capacitances > 100 pF

The circuit is as shown in Figure 2.5. High voltage was supplied through protective resistor to terminal “a” from a power unit. The rotating charger, consisting of two insulated metal

balls, transferred the high voltage gradually to the discharge capacitor which connected to the electrodes mounted to explosion vessel. In this way, the transferring charge rate could be controlled by varying the angular velocity of the rotating charger. Due to high values of the capacitors, the delay time, time before the spark occurred was often long. This lag of time could be reduced by placing radium capsules of various strengths into the test bomb. But in later work this was found potentially troublesome due to the caused slow leakage of electricity from the charged electrode before the breakdown.

Electric circuit with capacitances < 100 pF

In later work, the rotary charger was replaced by a Bakelite rod resistor of order of $10^{11}\,\Omega$. This high resistor rod had the same function as the rotary charger, and that was permitting a slow transfer of charge from the power unit to the spark circuit. The capacitors and the static voltmeter were now connected in parallel and used as a reservoir of known voltage, as shown in Figure 2.6. From this reservoir the voltage was charged to a desired potential, then isolated from the power unit and electricity was delivered to the test bomb through the Bakelite rod. The capacitance of the spark circuit could be adjusted down to 1 pF by means of the small extension capacitors and other devices.

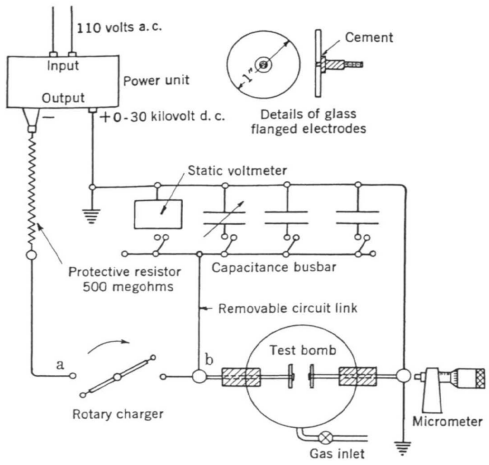

***Figure 2.5**: Scheme of apparatus for determining minimum ignition energies for electric-spark ignition. From Lewis and von Elbe (1961)*

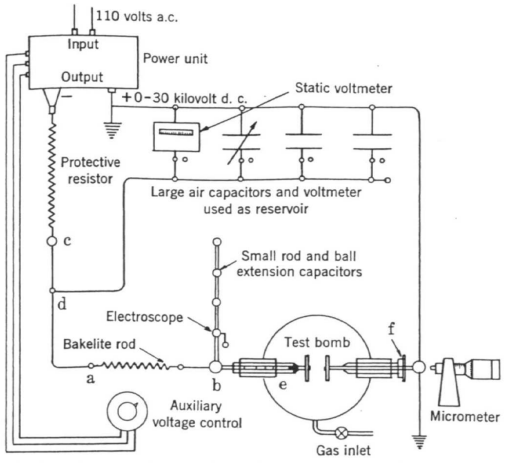

***Figure 2.6**: Apparatus arranged for spark circuit of very low capacitance .From Lewis and von Elbe (1961)*

2.2.4 Test method and statistical MIE criterion

After the desired spark gap was set, the explosion vessel was filled with a gas mixture of the desired composition. The electrode and the capacitor system was slowly charged and the voltage, U, at which the spark occurred was recorded. If the mixture did not ignite, the capacitance was increased by trial and error until the critical capacitance, C, for ignition was found. The ignition energy was calculated by the formula $E = ½ CU^2$, where U was the voltage just before spark discharge and C the energy storage capacitance.

It has not been possible to trace the statistical method used by Levis and Elbe for deriving MIE from the experimental data, but according to Moorhouse *et al.* (1974), their criterion was an ignition probability of only 1 %.

2.3 THE ASTM METHOD

2.3.1 Overview

The standard test method for MIE and QD in gaseous mixtures from ASTM (2007) is based on the Bureau of Mines/Lewis and von Elbe method. The method is applied to mixtures of specified fuels (gases and vapours of liquids) with air. The mixing ratio is varied from the most easily ignitable mixture to mixtures near to the flammable limit compositions. The breakdown voltage of the spark gap follows Paschen's law, which means that it depends on the gas mixture pressure, spark gap distance and the gas mixture composition.

With this standard test method, the expected accuracy is ± 10% in minimum ignition energy for MIE and ± 2% for QD. For mixture compositions near the flammable limits, the MIE increased rapidly as the flammable limits are approached and hence the standard deviation of ±10% does not apply here.

2.3.2 Test apparatus

The recommended reaction chamber is 1 dm^3 spherical stainless steel vessel of inner diameter (125mm). The 1.6 mm diameter metal electrodes shall be flanged with glass plates. The glass flanges should have a diameter of 5 to 10 times the electrode gap and a thickness of 2.38 - 3.18 mm.

For maximum testing flexibility, a DC power supply that can deliver 1-30 kV is recommended.

2.3.3 Electrical spark generation circuit

Figure 2.7 shows the electrical spark generation circuit of ASTM. The energy storage capacitance is in the range of 8-12 pF. A large isolating resistor is placed at the power supply terminal, and the other divider resistor at the bomb energy storage capacitance. For most ignitable mixture, the desirable value of the isolating resistor is 10^{12} ohms. For less easily ignitable mixtures, the resistance values are reduced inversely as the energy storage capacitance is increased.

Usually an electrostatic voltmeter is used to measure the spark gap voltage at breakdown. If the voltmeter has a capacitance greater than the energy storage capacitance, then a static voltmeter is used in conjunction with a voltage divider network. The divider resistor should be at least 10^{14} ohms.

The time constant, T (s), of the resistive-capacitive charging circuit equals T = RC where T and R is the resistance (Ω) and C the capacitance (F).

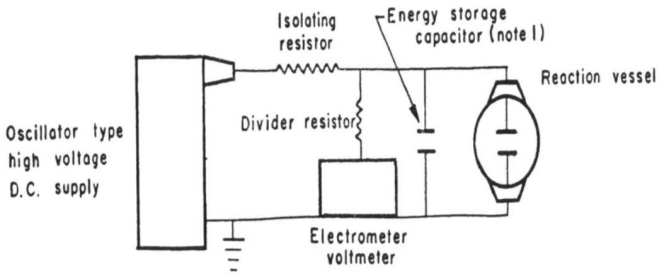

Figure 2.7*: Block electrical diagram. Note 1: distributed capacitance must be considered as part of the energy storage capacitance. From ASTM (2007)*

2.3.4 Test method and statistical MIE criterion

When the spark gap is set, the gas mixture to be tested is loaded into the explosion vessel. The voltage is then increased gradually until the breakdown voltage is reached and the spark discharge occurs. The spark energy is varied by varying the capacitance of the spark circuit.

The spark energy E is calculated as usual by the formula $E = ½ CU^2$ where C is the capacitance (F), U the spark voltage (V) and E the spark energy (J).

It is important to notice that there is no information or guidance as to the statistical analysis of the primary test data in this standard. No guidance regarding the number of

tests to be done at each spark energy level and the probability of ignition to be associated with MIE is given.

2.4 THE STUDY OF MOORHOUSE *ET AL.*

2.4.1 Overview

Moorhouse *et al.* (1974) determined the MIEs for C_1 to C_7 hydrocarbon/air mixtures. They also investigated the dependence of MIE on initial pressure and temperature. Their conclusion seemed to support the results reported by others. They found that MIE decreased with increasing temperature and pressure of the unburned gas mixture.

It is interesting to note that the MIE values reported by Moorhouse *et al.* were generally significantly higher than those reported by Lewis and von Elbe (1961). For example, the reported MIE of propane/air at ambient conditions and at optimal propane concentration of 5.3 vol. % was 0.46 mJ, whereas the value reported by Lewis and von Elbe (1961) was only 0.25 mJ.

2.4.2 Test apparatus

The stainless steel test vessel was a cylindrical with a diameter of 50 mm and length of 200 mm. The vessel was fitted with diametrically opposite 1.0 mm diameter tungsten electrodes. One of the electrodes could be moved to vary the electrode spacing and its position measured by a dial micrometer.

2.4.3 Electrical spark generation circuit

Based on the technique of Cheng (1967), the sparks of Moorhouse *et al.* (1974) were generated by means of the variable air capacitor device as illustrated in Figure 2.8. The capacitor consisted of two parallel plates, each 100x200 mm. The fixed plate was connected to the high-voltage electrode in the explosion vessel and the movable plate connected to the other earthed electrode. When the fixed plate had been charged from a high voltage source, the spring loaded movable plate was released and opened from its closest separation to the fixed plate (about 1 mm). The distance between the plates was increased rapidly. This caused a decrease of the capacitance and a corresponding increase of the voltage across the capacitor, and hence across the spark gap. A discharge between the electrodes occurred when the plate separation had caused a sufficient rise in voltage.

By using a displacement transducer, the position of the movable plate at the moment of spark-over could be determined, and hence the capacitance at spark-over. A small loop of wire around the input lead was also used as a capacitance voltage divider to give an indication of instant of discharge. The voltage of the charged fixed plate was measured by a decoupled electrostatic voltmeter.

This circuit essentially behaved as a simple capacitance discharge circuit with a very low inductance of about 1 µH. The external circuit resistance was also very low, about 2 µΩ. Therefore practically all the energy stored in the capacitor (½ CU^2) was deposited in the spark gap. The capacitance was in the range of 19-64 pF. The spark was equivalent to a damped oscillating wave of 9 MHz of about 1 µs duration.

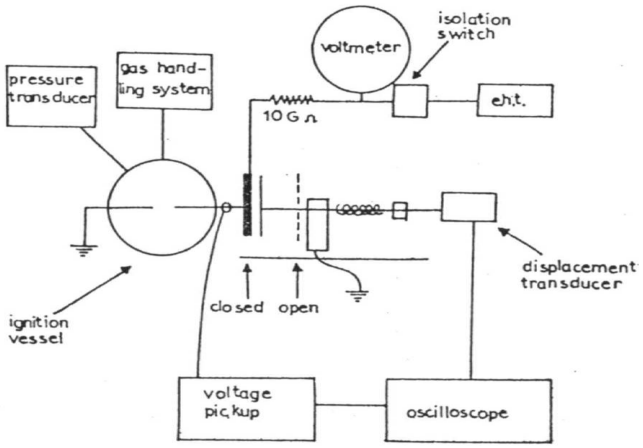

***Figure 2.8**: Diagrammatic representation of the expanding plate capacitor apparatus. From Moorhouse et al. (1974)*

2.4.4 Test method and statistical MIE criterion

Minimum ignition energies were determined by making up mixtures of known compositions and varying the spark energy until the borderline between ignition and no-ignition had been identified. Ignition was detected by means of a pressure transducer or by a voltage signal which indicated the occurrence of explosion or flame. For all experiments in their study, the electrode distance was set at 2.2 mm.

When the plates are separated, the voltage across the plates will increase and the capacitance of the plate system decrease according to the relation:

$$U_1C_1 = U_0C_0 \quad \rightarrow U_1 = \; U_0 \frac{C_0}{C_1} \tag{2.2}$$

Where U_0 and C_0 are the voltage and capacitance before plate separation, and U_1 and C_1 the voltage and capacitance at spark-over. C_1 was determined by the measurement of the plate distance at spark-over.

The energy in the spark is:

$$E = \tfrac{1}{2} C_1 U_1^2 \qquad (2.3)$$

By inserting equation 2.2 in 2.3, one gets:

$$E = U_0 \frac{C_0^2}{2C_1} \qquad (2.4)$$

The spark energy E in this study was calculated by using equation 2.4

Moorhouse *et al.* determined the MIE by just drawing the highest possible boundary line through the array of all the experimental ignition and no-ignition points, which had only no-ignition points below it. Figure 2.9 shows the points above the boundary line consist of both ignition and no-ignition points.

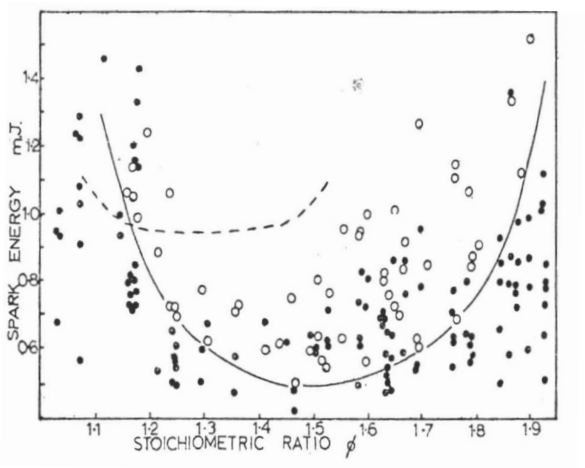

Figure 2.9*: Ignition diagram for n-pentane at 22 ºC, 2 atm, electrodes' separation: 2.2 mm; •, non-ignition; ₀, ignition. The results obtained at 0.75 atm are indicated by the broken lines. From Moorhouse et al. (1974)*

2.5 THE SYNCHRONIZED CAPACITIVE SPARK SYSTEM OF RANDEBERG.

2.5.1 Overview

In the circuit developed by Randeberg *et al.* (2006), a high voltage pulse was used for charging the capacitor instead of using a static high-voltage power supply. In this way, the moment of spark discharge could be determined precisely, which allowed synchronization with e.g. transient dust cloud generation. It was claimed that low-energy electric sparks in the range down to 0.03 mJ could be generated by using pointed electrodes, a spark gap of 1-2 mm and capacitance of a few pF. The main current pulse of sparks generated with this circuit were breakdown discharges of very short durations of below 100 ns.

Figure 2.10 shows the published results for minimum ignition energy of propane/air obtained by Randeberg *et al.* (2006). For the various gas concentrations studied considerable ranges of spark energies were obtained both within ignition and non-ignition. As can be seen from Figure 2.10, no non-ignitions were obtained in the gas concentration range between 4.0 and 7.0 vol. %, and hence no MIE could be determined. However, the results seemed to be supported by some data from Kono *et al.* (1976) and Parker (1985), indicating an MIE below 0.1mJ.

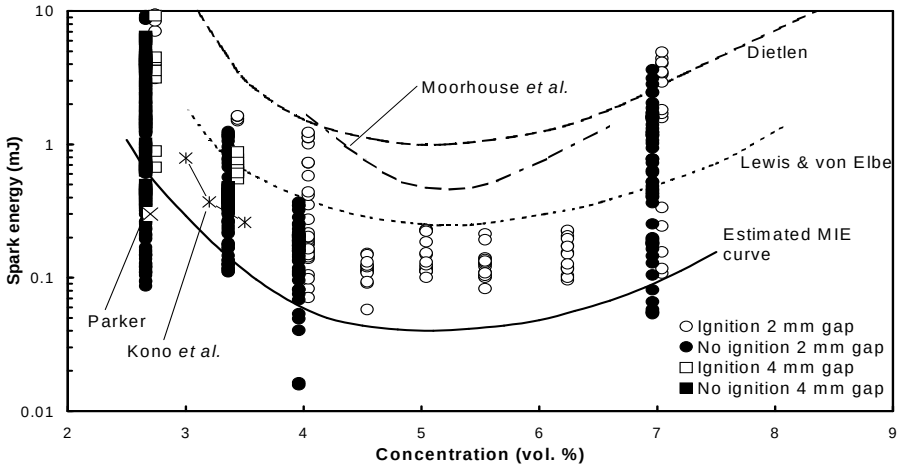

Figure 2.10*: Minimum electric spark energy for ignition of propane/air mixtures as a function of propane concentration. The data points are from Randeberg and Eckhoff (2007).*

2.5.2 The test apparatus

The cylindrical explosion vessel used in the experiments was similar to the Mike apparatus from Kühner. It had a diameter of 11.5 cm and a volume of 1.2 dm^3. To avoid

corona discharge prior to breakdown, the 2.0 mm diameter tungsten electrodes were rounded off to an angle of approximately 60°. The electrode gap widths were in the range from 1.0 mm to 6.0 mm.

With the aim to reduce the noise influence on the measuring probes, a shield with an integrated system for voltage and current measurement was placed around the combustion vessel. As can be seen in Figure 2.11, this measurement system was also integrated in the circuit.

2.5.3 Electrical spark generation circuit

A primary capacitor of 1 µF was charged to a voltage of about 300 V. By triggering the thyristor, this capacitor would be discharged into the primary coil of a high-voltage transformer and a pulse of about 15 kV was generated in the secondary windings of the transformer. The high-voltage pulse had a rise time of about 0.7 ms and was supplied to the discharge capacitor through a charging resistor. This produced a corresponding voltage build-up on the discharge capacitor. When the breakdown voltage of the electrode gap was reached, the energy in the discharge capacitor was delivered to the spark gap.

To avoid recharging of the discharge capacitor during the spark discharge, the time constant RC (where R was the charging resistance and C the discharge capacitance) had to be at least 1 µs. Typical values of R were then between 100 kΩ and 1 MΩ, depending on the size of the discharge capacitor. The spark discharge times were less than 100 ns.

The schematic layout of the spark discharge circuit is shown in Figure 2.11

Randeberg assumed that no further energy than that stored in the discharge capacitor was delivered to the spark gap. As discussed in 2.5.5, this assumption as not valid. In the present study, an improved version of the Randeberg *et al.* generator was developed and repeated ignition tests with propane/air were performed.

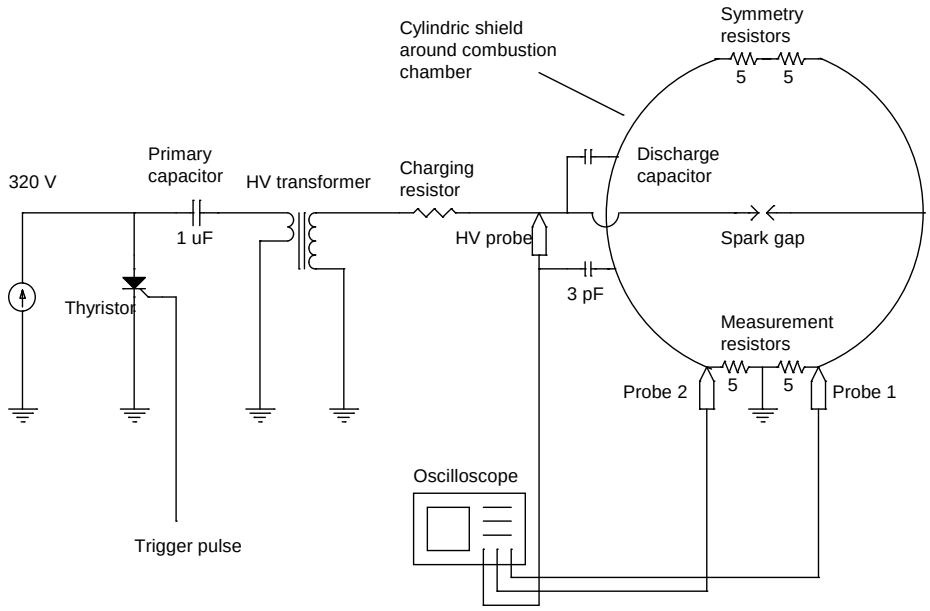

***Figure 2.11**: Schematic layout of the spark discharge circuit and the integrated spark energy measurement system.*

2.5.4 Determination of spark energy

Ignition tests were performed in series of ten successive trials at each energy level. The net spark energy in each trial, E, was calculated by the following equation:

$$E = \int Ui\, dt - \int R_M i^2\, dt \qquad (2.5)$$

Where U and i are the instantaneous spark voltage and current, measured across the spark gap during the life time of the spark pulse. The second term is the energy lost to the measurement resistors.

The spark voltage as a function of time was measured by using a high-voltage probe. This probe had a capacitance of 3 pF and had to be taken into account for calculation of the total capacitance involved in the discharge. The current was measured by two independent probes to reduce the noise influence (which was pronounced for the low spark energies).

2.5.5 Further investigation about MIE of propane/air based on the work of Randeberg

With the aim to reduce the additional energy supply to the spark after discharge of the discharged capacitor, Eckhoff *et al.* (2008) modified the circuit of Randeberg *et al.* (2006). They pointed out that the circuit did allow a small current of about 1/1000 of the peak current of the first pulse to continue to flow through the spark gap, after the main pulse from the discharge capacitor has ended. This current had a value of around 20-50 mA and lasted up to 100 μs, which corresponded to a substantial additional amount of energy of more than 1 mJ. The real spark energies in the experiments by Randeberg and Eckhoff (2007) were much larger than those quoted in their paper. Therefore this recent investigation did not support the earlier published results of MIE value for propane/air below 0.1 mJ.

2.5 MIE STUDIES BY OTHER WORKERS

2.5.1 The study of Calcote *et al.*

Calcote *et al.* (1952) used almost the same apparatus and procedure as used by Lewis and von Elbe (1947) to determine MIE of a large number of fuel types, employing stoichiometric fuel/air mixture at a pressure of 1 atm. With this circuit, a known (3000 to 4000 pF) capacitance in parallel with the spark gap was charged through a high resistance of value 10^9-10^{12} Ω until a spark occurred. 4.9 mm stainless steel hemisphere electrodes were used. With the aim to reduce the spark breakdown lag and ensuring a constant breakdown voltage at given electrode distance, the electrodes were irradiated with ultraviolet light.

The MIE results for most gases from their work were in good agreement with data of Lewis and von Elbe. At stoichiometric concentration, the values for some gases, including propane, were slightly lower than those reported by Lewis and von Elbe.

2.5.2 The studies of Kono *et al.*

Kono *et al.* (1976) investigated MIE of lean propane/air mixtures related to optimum spark durations by using composite spark, consisting of a short capacitive discharge of 0.5 μs and an inductive discharge of much longer duration. The spark energy was therefore calculated as a sum of the capacitance spark energy of the first short pulse and the integrated power of the secondary inductive component. The electrodes used in their

experiments were 30° half cone tungsten wire of 0.3 mm diameter, separated in a distance nearly equal to the quenching distance of the mixture.

Their study showed that the minimum ignition energies varied greatly with spark duration and had minimum values when the spark duration was at optimum. At durations above and below the "optimum", the ignition energies were increasing. According to Kono *et al.* (1992), the MIE for short spark durations increased due to the heat loss to the unburned gas stream that cooled the flame kernel and the energy was taken away by the shock wave. For long spark durations, the flame kernel remained near the spark gap, so that the heat loss from the flame kernel to the spark electrode increased with increasing spark duration. Spark energy supplied after the critical size of the flame kernel was formed (a few hundred μs) would not contribute to ignition process, but only increase the overall ignition energy.

Figure 2.12 shows that the optimum spark duration for 3.0-3.5 vol. % propane/air mixture is in the order of 50 μs. Even with 50% ignition frequency criterion, their lowest minimum ignition energies were less than half of those which were reported by Lewis and von Elbe (1961).

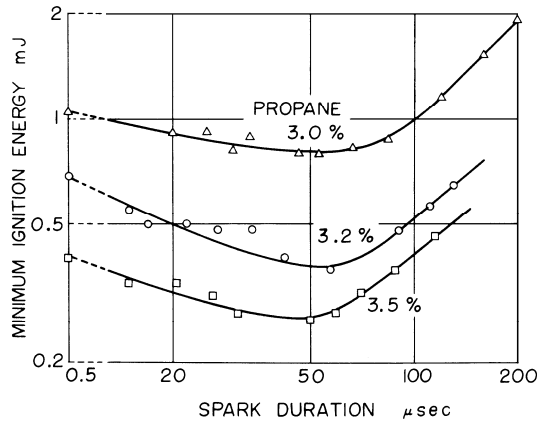

Figure 2.12*: The effect of the spark duration on the minimum ignition energy for gap width nearly equal to quenching distance. From Kono et al. (1976).*

Knowledge about the flame kernel growth combined with MIE data provides a better understanding of spark ignition. Kono *et al.* (1992) showed the influences of the electrodes' configuration and spark duration on the flame kernel structure. A short summary of their work is given in appendix A.

2.5.3 The study of Parker

With the same aim as Kono *et al.* (1976), Parker (1985) also studied the influences of discharge duration on the MIE for lean propane/air mixture. His pulse forming network consisted of an arrangement of capacitors and inductors ("transmission line"). Parker obtained well defined rectangular voltage and current pulses. The produced arc discharge

had energies values of 0.1 to 20 mJ and durations in the range of 0.2 to 100 µs. The spark energy was defined as the integral of power versus time across the spark gap. MIE was defined as the spark energy giving an ignition probability of 10%. Parker used 0.5 mm diameter electrodes in 3 different gap widths 2.0, 4.0 and 7.0 mm to study MIE in relation to spark duration.

Parker found a strong dependence of MIE on the spark duration. MIE increased significantly when spark duration was increased from 0.2 to 100 µs. With a 4.0 mm spark gap, Parker found a MIE value of 0.3 mJ for 2.7 vol. % propane/air. This value cannot be compared directly with Lewis and von Elbe's data since their lowest experimental concentration for propane/air was 3.0 vol. %.

2.5.4 MIE determination by using laser "sparks"

Generally, the MIE values obtained for propane/air by using laser sparks are higher than data obtained with electrical sparks. Lee *et al.* (2001) used a laser spark ignition system to study the MIE values of hydrocarbon fuels in air at a range of pressures and equivalence ratios. For 5.0 vol. % propane/air, they found a MIE of about 0.6 mJ. This is considerably higher than the value of 0.25 mJ, given by Lewis and von Elbe (1961), but not much higher than 0.48 mJ found in the present investigation using the ASTM apparatus.

It's important to emphasize that these differences between the MIE values are not just due to the different measurement techniques, but also to different criterions of ignition probability chosen to define MIE with.

2.7 STATISTICAL ANALYSIS OF SPARK IGNITION

Eckhoff (1970) pointed out that the term minimum ignition energy must be associated with a certain ignition probability; otherwise it would be difficult to compare the obtained values of MIE.

One question that arises is: What level of probability is most appropriate to use? A second question is: How many trials are required to achieve a true or reliable ignition probability?

Ko *et al.* (1991) suggested that a probability of ignition of 50 % would be an appropriate choice. In many experimental studies, ten trials at each energy level have been used. But some workers emphasize that this sample size is too small to obtain sufficiently accurate determination of the true probability. When discussing the theory of Bernoulli's trials, Eckhoff (1970) mentioned even sample sizes of 20 trials might not be large enough to give the required accuracy in the determinations of the true probability of ignition.

Due to the statistical nature of spark discharges, breakdown occurs at different instantaneous voltages even when apparently identical test conditions are applied. The representative value of breakdown voltage would be the calculated arithmetic mean:

$$U_{break\,(mean)} = \frac{1}{n}\sum U_{break} \tag{2.6}$$

Here n is the number of spark discharges and U_{break} the breakdown voltage. But this may lead to an untrue value of minimum ignition energy because for achieving high accuracy of the results, it often requires a large number of tests, n.

It is also reasonable to state that the ignition probability, P, of a given combustible mixture increases with increasing spark energy. The probability of ignition P is denoted as the ratio of the number of ignitions, m is the total number of spark discharges in the total number of tests, n.

$$P = m/n \tag{2.7}$$

Moffett *et al.* (2007) re-emphasized that there is no single threshold energy value, but a distribution of the probability of ignition versus spark energy. They applied logistical regression for binominal outcomes to analyze the results of spark energies near the reported MIE, where the energy levels for ignition and no-ignition results overlap. The result was S-curve with ignition probability as a function of spark energy, with 95% confidence envelope is shown in Figure 2.13. Spark energy levels where only no-ignition or ignition are obtained have ignition probabilities of 0 and 1 respectively. In the following, E denotes MIE for a given probability P of ignition.

Based on the logistic regression model the probability of ignition, P(E), for a given spark energy, E, can be calculated by the following equation:

$$P(E) = \frac{1}{1+e^{-\beta_0-\beta_1 E_i}} \tag{2.8}$$

Where β_0 and β_1 are coefficients estimated by maximizing the likelihood function.

With the known parameter, for a certain probability of ignition P(E), values of spark energy, E, can be calculated by:

$$E = (ln\frac{P(E)}{1-P(E)} - \beta_0) / \beta_1 \tag{2.9}$$

The disadvantage of equation 2.9 is E cannot be found when P(E) = 1.0, because the natural logarithm of 0 would be negative infinity. However, the equation is applicable to any value close to unity.

The upper confidence limit (UCL) and lower confidence limit (LCL) for the 95% confidence interval for E can be estimated by:

$$UCL/LCL = E \pm z_{\alpha/2} \sqrt{(\sigma_{00} + 2E\ \sigma_{01} + E^2\sigma_{11})/\beta_1^2} \quad (2.10)$$

Where σ_{00}, σ_{01} are the variances and σ_{11} is the covariance of β_0 and β_1. α for 95% confidence interval is 0.05 hence $z_{\alpha/2}$ is the z value from a standard normal distribution. The covariance of β_0 and β_1, σ_{11} is the product of correlation factor, ρ and standard deviations of β_0 and β_1.

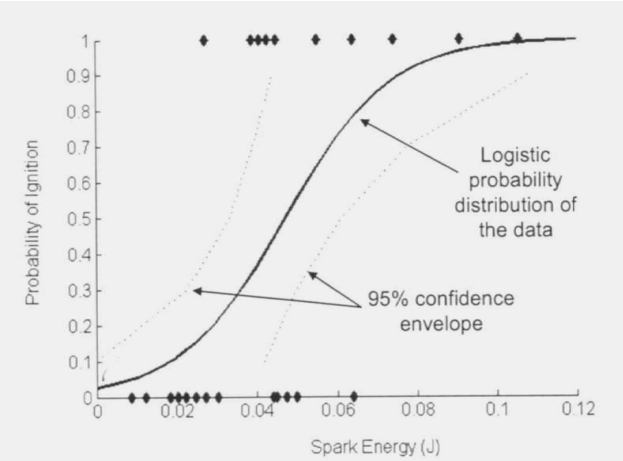

Figure 2.13*: Logistic probability distribution and 95% confidence envelope for Jet A spark ignition data. The original data points are also plotted in the diagram. As in any binominal outcome model, y=1 for a "success"(in this case is ignition) and y=0 for a "no success"(no-ignition) for a given spark energy. From Muffett et al. (2007).*

CHAPTER 3: METHODS AND APPARATUSES USED IN THE PRESENT WORK

3.1 THE ASTM METHOD

3.1.1 Overview

With the aim to qualify the results of MIE determined by using an improved version of synchronized spark generator of Randeberg *et al.* (2006), which will be described later in section 3.2, it was decided to construct a copy of the standard ASTM spark generator for MIE determination of gases, and determine MIE of propane/air.

3.1.2 The test apparatuses

In the present experimental work, following apparatuses were used:

- Explosion vessel with glass flanged electrodes. Spark gap length 2.0 mm.
- Trek Model 542-2 electrostatic voltmeter
- Capacitors of different values
- High voltage supply with range up to 20 kV

The propane concentration in the mixture was measured by using oxygen analyzer (Servomex 1100). The descriptions of the apparatuses and the gas mixing system are given in section 3.3 and Appendix B.

The distance between the electrodes was set to 2.0 mm by using leaf gage of known thickness and the spark energies varied by varying the capacitor's values (14-100 pF).

3.1.3 The electrical spark generation circuit

A spark discharge circuit was constructed based on the circuit of the ASTM described in section 2.3. Figure 3.1 shows a high-voltage power supply connected to charging a $1x10^{12}$ Ω resistor. A capacitor and an electrostatic voltmeter were connected directly across the spark gap.

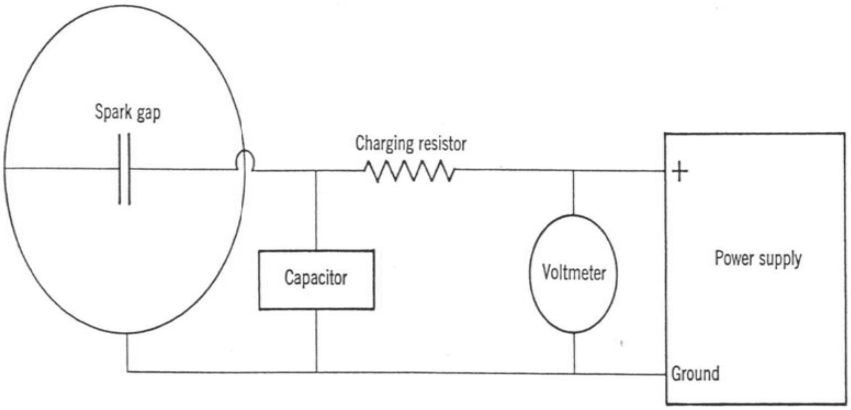

Figure 3.1*: Block diagram of the electric spark circuit of ASTM for determination of MIE for gases and vapours. From Litchfield (1967)*

3.1.4 Determination of spark energy

After the gas mixture of the desired concentration has been loaded into the explosion vessel, the applied voltage across the spark gap was increased gradually until a sparks occurred.

Some introduction experiments were performed with the aim to find the spark breakdown voltage in air for 2.0 mm spark gap length. According to Babrauskas (2003), for a spark gap distance of 2.0 mm the breakdown voltage is around 6.0 kV. Due to the statistical nature of spark discharges, the breakdown occurs at different voltages even for apparently identical test conditions. In the present work, the breakdown voltages for the 2.0 mm spark gap were in the range of 6.0-7.0 kV.

The spark energy E was calculated by:

$$E = ½ CU^2 \qquad (3.1)$$

Where C is the energy storage capacitance, the sum of the capacitance of the electrode gap and the stray capacitance. U is the spark voltage at the moment of discharge, measured by a Strek- electrostatic voltmeter. C and U have the standard units of F (Farad) and V (Volt). This yields E in J (Joule). In the present work, the stray capacitance is estimated to be about 2.0 pF.

3.2 THE NEW SYNCHRONIZED SPARK GENERATOR METHOD

3.2.1 Overview

Randeberg *et al.* (2006) described a spark generator, which was claimed to be able to produce synchronized capacitive spark discharges of low energies down to 0.03mJ. However, Eckhoff *et al.* (2008) re-examined the discharge circuit of Randeberg *et al.* and concluded that the real spark energies in the experiments by Randeberg and Eckhoff (2007) were much larger than those quoted in their paper. In fact, the additional energy was of order of 1 mJ. Figure 3.2 shows the pulse generated by the synchronized spark generator of Randeberg *et al.*, as described by Eckhoff *et al*..

In the present investigation, an improved version of the synchronized spark generator of Randeberg *et al.* has been constructed. The aim of the improvement has been to minimize the additional energy contribution to the effective spark energy. Figure 3.3 shows the pulse produced by the new synchronized spark generator. At spark discharge, the pulse over the spark gap is as shown in Figure 3.4.

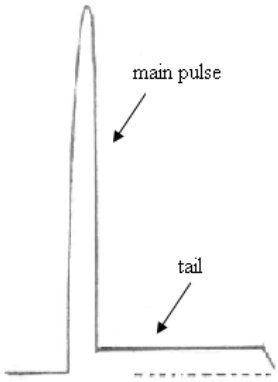

***Figure 3.2**: Pulse produced by the synchronized spark generator of Randeberg et al. (2006). The main pulse has duration of about 100 ns and peek voltage of about 6 kV. The tail of the pulse has voltage of about 650 V and duration of 50-100 µs.*

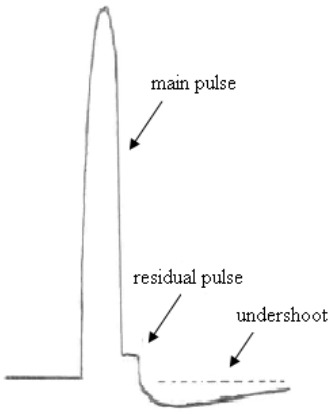

***Figure 3.3**: Pulse produced by the new spark generator. The 2-3 µs main pulse has a voltage of about 10 kV. The residual pulse has a voltage of about 650 V and duration from 1 to 3 µs.*

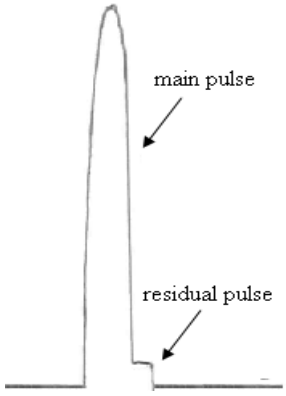

***Figure 3.4**: Pulse produced by the new spark generator. At spark discharge, the undershoot of the pulse from Figure 3.3 is eliminated.*

3.2.2 Test apparatuses

The experimental set-up consisted of the following apparatuses:

- Explosion vessel with glass flanged electrodes. Spark gap length 2.0 mm.
- Capacitors of different values
- Voltage supplies
- High voltage probe Tektronix P6015, P6015A and P6013A
- Philips pulse generators, PM 5705 and PM 5715.
- Tektronix TDS 3034B oscilloscope

Propane concentration in the tested mixture was measured by a Servomex 1400 gas analyser, based on infrared light absorption. For the descriptions of the apparatuses and the gas mixing system used in this experimental work refer to section 3.3 and Appendix B.

3.2.3 Electrical spark-generation circuit

Figure 3.5 illustrates the experimental setup of a new synchronized spark-generation circuit. The circuit has been developed by senior engineer Werner Olsen at UoB, Department of Physics and Technology. The detailed circuit diagrams of the different sub-circuit in Figure 3.5 are given in Appendix C.

When the system is triggered, the pulse generator P1 generates two tailored pulses of 60 µs duration 240 µs apart. The first pulse then triggers pulse generator P2, whereas the second pulse triggers pulse generator P3.

The pulse from pulse generator P2 is a 0.24 V rectangular pulse of 260 µs duration, which passes through amplifier A1 before entering the primary windings of the high voltage transformer T1. Figure 3.6a illustrates a typical output signal from T1. The simple diode circuit F1 filters out the first negative part of the pulse. The second positive part of the pulse has a peak voltage of about 400 V and for the simplicity of later description this pulse is called pulse I.

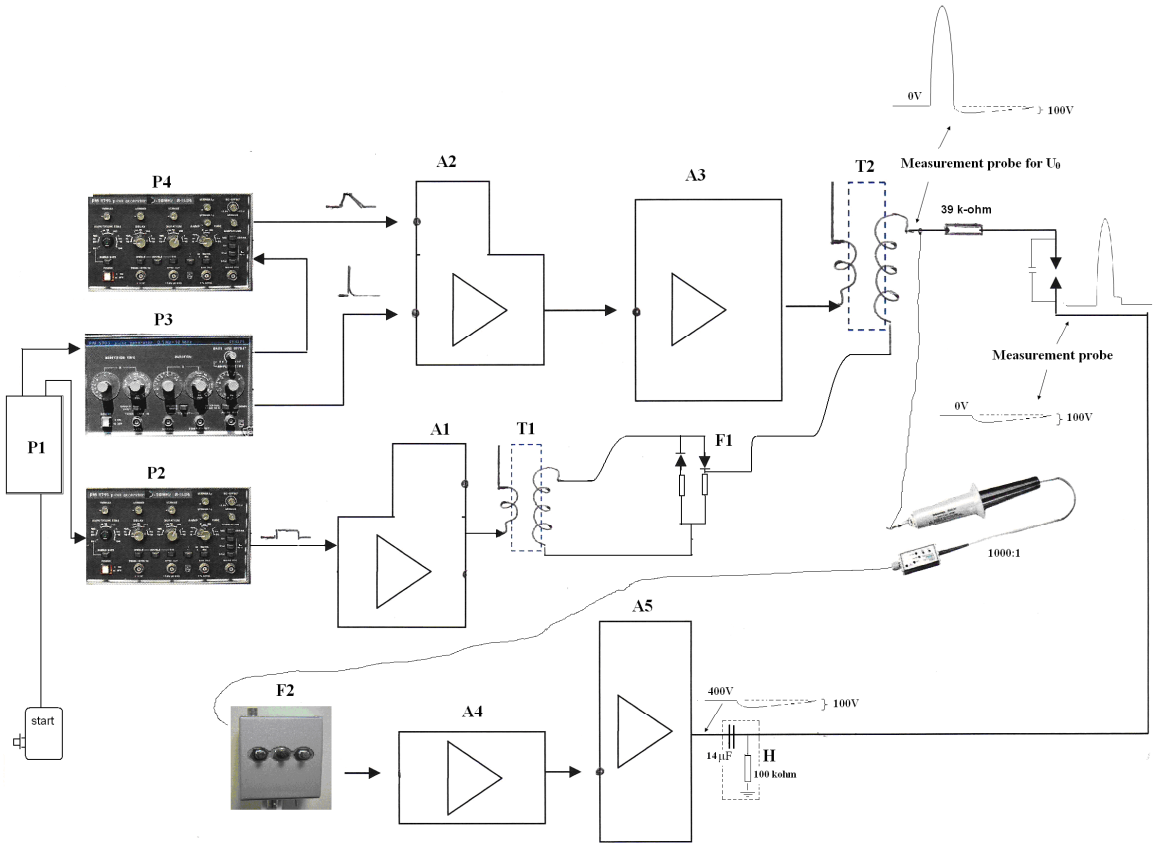

***Figure 3.5**: Schematic block diagram of the improved version of the synchronized spark generator of Randeberg et al. (2006). A1-A5 are the amplifiers. T1 and T2 are high-voltage transformers. P1 is a tailor-made pulse generator. P2 and P4 are Philips pulse generators PM5715. P3 are Philips pulse generator PM 5705.*

The output from pulse generator P3 is a short-duration (0.06 µs) pulse with amplitude about 13V, which triggers pulse-generator P4 that produces a low voltage pulse (2.5V) of 8.0 µs duration and rectangular shape as illustrated in Figure 3.6b.

The pulses produced by P3 and P4 are both sent to amplifier A2, where they are amplified about 7.5 times and combined to one signal. Figure 3.6c shows the dual-peak signal from amplifier A2. The first peak originates from the pulse generated by P3 and is now about 90V. The second peak originates from the signal from P4 and is now about 19 V.

The dual-peak signal illustrated in Figure 3.6c enters amplifier A3 where it is inverted by a NPN transistor and the amplitude amplified from 90 to about 500 V. Figure 3.6d shows the two-peak pulse from Figure 3.6c has now become a single peak pulse with a “knee”.

The pulse from amplifier A3 is sent to the high-voltage transformer T2. A diode is introduced in the circuit to minimize the amplitude of the undershoot. With the aim to

shorten the duration of the high-voltage pulse, the iron core of the high-voltage transformer in this circuit is replaced by ferrite core. Figure 3.6e shows the pulse is transformed to a single-peak high-voltage pulse of about 10 kV and duration about 4-6 µs. The amplitude of the undershoot is about 500 V. This pulse signal is then combined with pulse I (+ 400V) to produce a final undershoot of about 100V.

Due to the high-voltage sensitivity of diode, the pulse signal of 10 kV and undershoot of 100V are then reduced by a factor of 1000 by the mean of a Tektronix P6015 high-voltage probe. It appears that it would be more appropriate reduce the voltage by a factor of 100 or 200, but in the present work, a factor of 1000 was used due to the availability of the high-voltage probe.

Filter F2 eliminates the 10 kV peak of the pulse-signal after it has been reduced to a 10V peek pulse. The remaining undershoot is sent to amplifiers A4 and A5. The aim is to amplify it 1000 times to recover its original shape and amplitude, so that the undershoot from both sides of the spark gap can eliminate each other.

The function of the RC-circuit H is to offset the DC level.

By placing two high-voltage measurement probes as shown in Figure 3.5, the shapes and magnitudes of the pulses from both sides of the spark gap and spark occurrence are recorded by the mean of a Tektronix TDS 3034B oscilloscope.

Figure 3.6f shows the pulse signal at spark discharge. The main pulse would be about 10 kV, with duration 2-3 µs.

Prior to spark discharge, the voltage gradually increases until the spark occurs and then drops rapidly to 0. However, the residual part of the input pulse causes the voltage to increase and stabilize at about 600- 650 V. This resulting additional energy supply is denoted as the residual pulse and has a duration about 1-3 µs, depending on when the spark gap breakdown occurs.

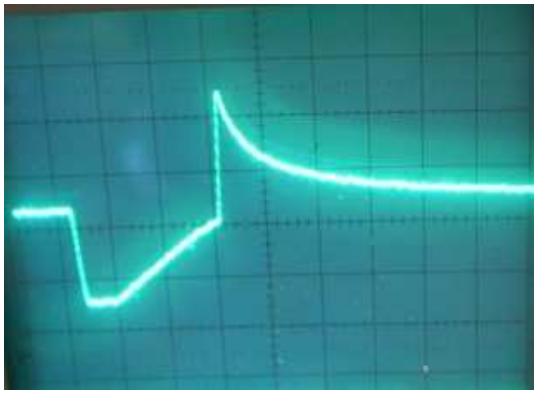

Figure 3.6a: Pulse generated by P2 after it has entered amplifier A1 and transformer T1.

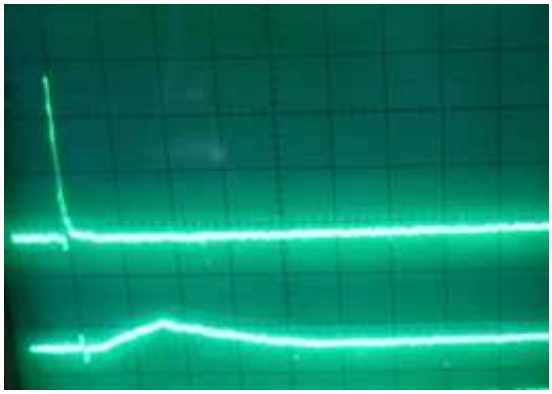

Figure 3.6b: Pulse-signals generated by Philips pulse-generators P3 and P4.

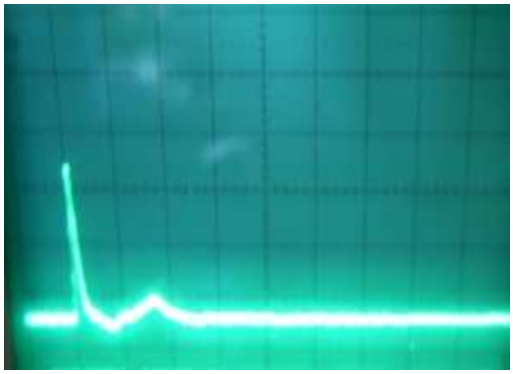

Figure 3.6c: The pulse signal from amplifier A2. The first peek has a voltage value of about 90 V and the second of about 19V.

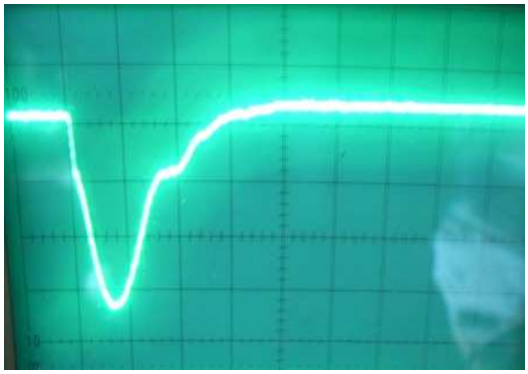

Figure 3.6d: The negative pulse-signal with positive overshoot from amplifier A3. The voltage peek is about (-) 500 V and the positive overshoot (+) 60 V.

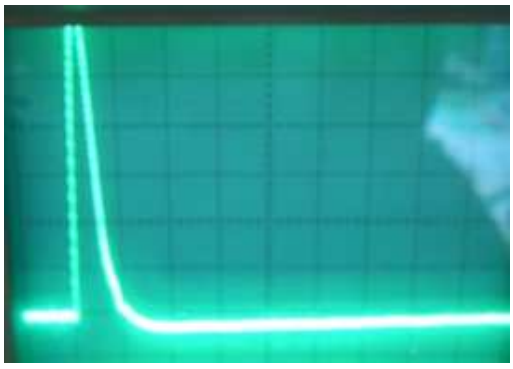

Figure 3.6e: The pulse-signal prior to downscale 1000:1. The voltage-peek is about 10 kV and undershoot 100V.

Figure 3.6f: The pulse-signal at spark discharge.

Figure 3.6: *Pulse-signals at various stages of pulse shaping in the new improved spark generator based on that of Randeberg et al. (2006).*

3.2.4 Determination of spark energy

The same flanged electrode system as used in the ASTM test was used. The spark gap was set to 2.0 mm. After the explosion vessel had been filled with gas mixture of the desired concentration, the spark generator was triggered. If the spark triggering is not successful at first trail, triggering is repeated with 15-20 s intervals until the spark occurs. The 15-20 s interval is necessary to ensure that the energy supplied by the preceding pulse has dissipated. The spark energy is varied by varying the value of the connected capacitor.

The spark energy E was calculated by:

$$E = E_1 + E_2 = \tfrac{1}{2} C U_1^2 + \int U_2 i \, dt \qquad (3.2)$$

Hence the first term E_1 is the energy contained in the main pulse, C being the storage capacitance and U_1 the voltage at spark gap at the moment of breakdown. The stray capacitance is estimated to be about 2 pF and must be included in the storage capacitance for the calculation of E_1. The second term E_2 is the additional energy contribution from the residual pulse. U_2 is the voltage and i the current. The duration of the residual pulse i.e. the duration of the additional energy to the spark channel varies from 1 to 3 µs, depending on the time when the spark occurs.

When the input voltage U_0 to a RC-circuit is known, the output voltage U_1 can be calculated in accordance with the analogue-block-diagram illustrated in Figure 3.7. The discharge voltage U_1 is then estimated by following equation:

$$U_1 = \frac{1}{RC} \int (U_0 - U_1) \, dt \qquad (3.3)$$

R being the resistance and C the capacitance connected to the spark gap. U_0 is the pulse voltage measured by placing the high-voltage probe upstream of the spark gap as shown in Figure 3.5.

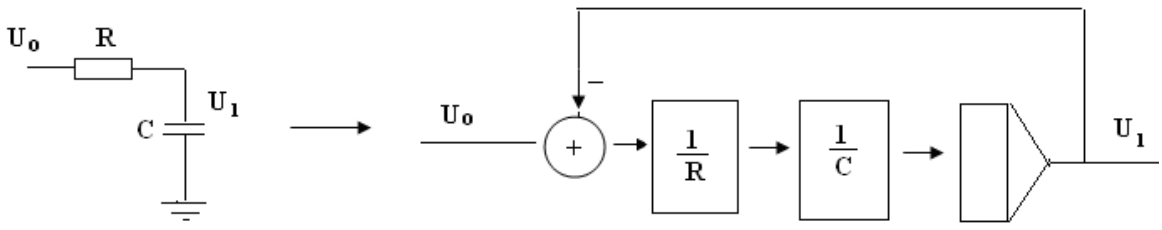

Figure 3.7: *Analogue-block-diagram of the RC-circuit*

The current i in the residual pulse is estimated by:

$$i = \frac{U_1 - U_2}{2R} = \frac{U_1 - 650}{2R} \quad (3.4)$$

Equation 3.4 shows that i is the average current, strongly influenced by the discharge voltage U_1 and the resistance R connected to the spark gap. Based on the work of Kleppa (2008) and the present work, U_2 has value of about 600-650 V. In the present calculations, the value 650 V was used. For a typical discharge voltage U_1 of 10 kV, the current i in the residual pulse has a value of about 0.12 A when a 39 kΩ resistor is inserted prior to the spark gap. By increasing the resistance to 110 kΩ, i decreases to 0.04 A.

3.3 APPARATUSES

3.3.1 The explosion vessel

Figure 3.8 shows the cross section of the explosion vessel used in the present work. The reaction vessel is a cylindrical hard plastic tube with inner diameter of 40 mm and height of 156 mm, corresponding to a net internal volume of 0.20 dm^3. The inlet tube with the valve is placed in the bottom and the outlet tube on the top of the explosion vessel.

Two 1.6 mm flat ended tungsten electrodes flanged with glass plates are located at the centre of the tube. One is fixed while the other is moveable, allowing adjustment of the gap distance between the electrodes. The electrode tips screw into stainless steel rods, which extends through the wall of the explosion vessel, allowing external electrical connections.

The glass flanges were made of borosilicate glass and have a diameter of 15 mm and thickness of about 3.0 mm. They were fastened to the electrodes with Araldite. A locking ring for fixing a paper cover is placed at the top of the vessel.

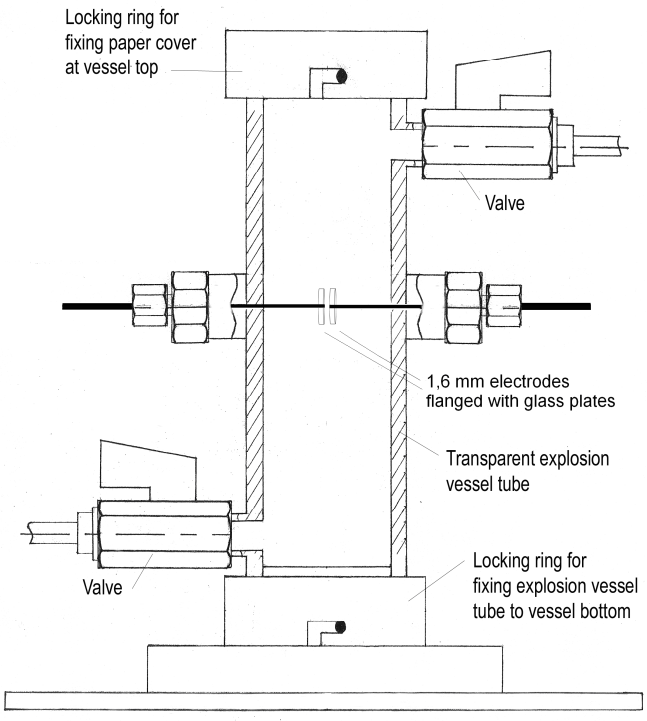

***Figure 3.8**: Cross section of explosion vessel with centrally located flanged electrodes*.

3.3.2 The electrostatic voltmeter

Trek Model 542-2 ESVM (electrostatic voltmeter) is a field meter. The model has a voltage detection and measurement range of 0 to ± 20 kV, a ± 5% reading inaccuracy, ± 0.2% of full scale. According Trek (2002), the reading accuracy can be improved by connecting a capacitor of value about 50-100 pF between the test surface and the explosion chamber. In the present work, it was decided that the reading inaccuracy of 5% was acceptable, because the extra connected capacitor would give other affects, causing other problems in considerations for the spark circuit and much slower reading was also observed.

Figure 3.9 shows the sensing probe is side viewing orientated, placed in a non-conductive holder with the probe positioned to allow the aperture to face the test surface.

According Trek (2002), a typical Trek round body, side-view probe, placed about 5.0 mm from the test surface would have a capacitive coupling around 2.0 pF. With the aim to protect the probe, a resistor of value 330 kΩ was connected to the test surface right before the electrical connection to the explosion chamber. The capacitance contribution from the probe to the discharge gap is therefore very small. The total stray capacitance and the capacitance of the probe in this circuit system was estimated to about 2.0 pF.

To prevent arcing between the measured surface and the probe, for the measurement of ± 10 kV, it is recommended that the probe should not place closer than 12 mm. In the present work the distance between the probe and the test surface is 6.0 mm. The test surface is a metal plate in circular form with diameter around 15 mm, placed up on a cylinder non-conductive holder.

The electrostatic voltmeter was first zero calibrated and then calibrated against a known DC- power supplier. The calibration showed that the electrostatic voltmeter is giving good readings. The results of the calibrations were plotted into diagrams and can be reviewed in the appendix B.

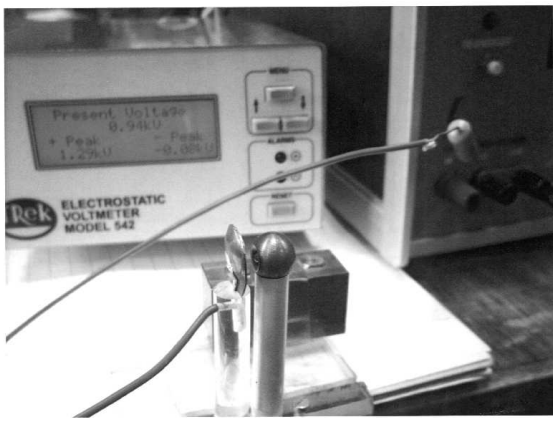

Figure 3.9*: Trek Model 542-2 ESVM with the probe and metal test surface in circular form*

CHAPTER 4: RESULTS AND DISCUSSION

4.1 RESULTS OBTAINED WITH THE ASTM CIRCUIT

4.1.1 Determination of MIE as a function of propane/air concentration

About 220 tests were done to determine the minimum ignition energy for propane/air. The propane concentration range covered was in the 3.5-8.0 vol. %. The main aim of the tests was to find the boundary between ignition and no-ignition across the investigated concentration range.

The spark energy values were calculated from equation 3.1 ($E = ½ CU^2$).

By using the same method for identifying the minimum ignition energy of Moorhouse *et al.* (1974), the highest possible border line was drawn through the array of experimental data points, below which there was no ignition point. In this way, the U-shaped curve shown in Figure 4.1 was obtained. The data points inside (above) the U-shaped curve contain both ignition and no-ignition data. The minimum of this U-shaped curve indicates a minimum ignition energy of about 0.50 mJ for propane concentrations in the range of 5.0-5.5 vol. %.

Figure 4.1 also shows that the spark gap distance of 2.0 mm used in the present work was the quenching distance for a propane concentration of about 4.2 vol. %. No ignition was observed for propane concentration lower than 4.2 vol. %, even if the spark energy was increased significantly. On the other hand, the present results do not indicate that 2.0 mm is the quenching distance for any specific concentration on the fuel rich side. The experimental results showed that ignition was still obtained by increasing the spark energy for mixtures up to around 8.0 % vol.

According to the study of Lewis and von Elbe (1961), see Figure 2.1 in section 2.1, the quenching distance should also be a U-shaped function of propane concentration. For a given pressure, every concentration of the mixture corresponds to a certain quenching distance. At ambient conditions (1 amt pressure), a spark gap of 2.0 mm seems to have a quenching effect for propane/air mixtures of around 4.0 and 6.0 vol. %.

The result obtained with the ASTM method in the present work was also compared with results reported by Moorhouse *et al.* (1974) and Lewis and von Elbe (1961). Figure 4.2

shows that the obtained MIE is twice higher than the result of Lewis and von Elbe, but is in very good agreement with the data of Moorhouse *et al.*.

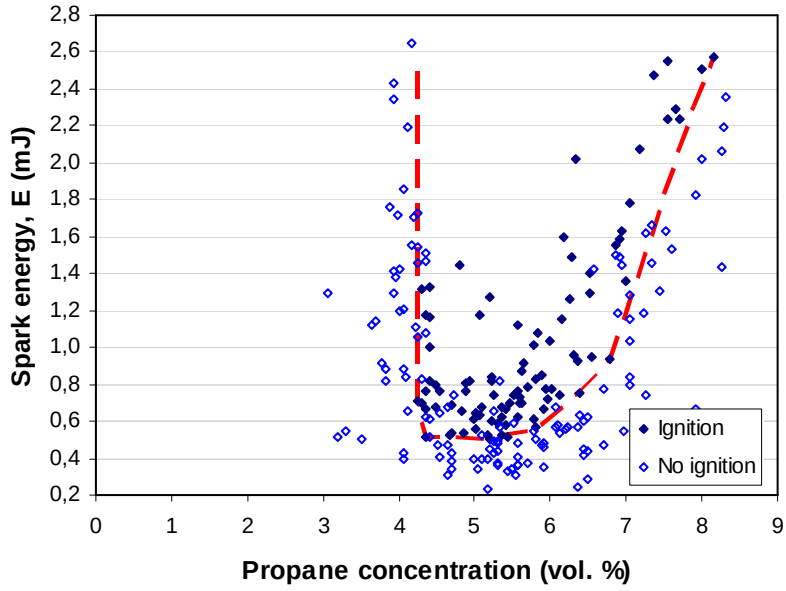

***Figure 4.1**: Minimum electric spark energy for ignition of propane/air mixtures as a function of propane concentration.*

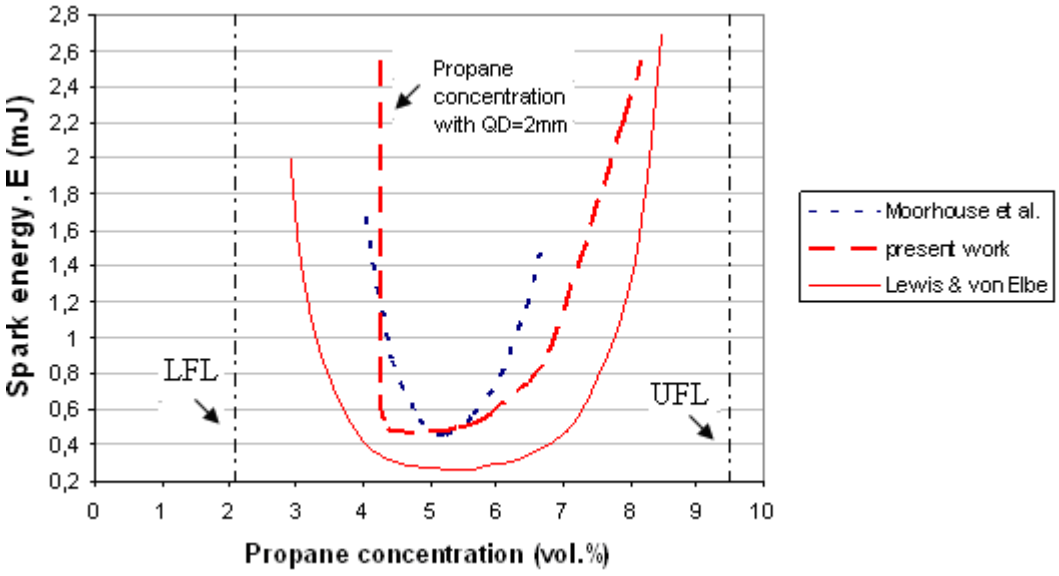

***Figure 4.2**: The minimum ignition energy for propane/air mixtures as a function of propane concentration. The obtained data of ignition energy based on ASTM in compared with the results of Moorhouse et al. (1974) and Lewis & von Elbe(1961). The lower (LFL) and upper (UFL) flammability limits for propane in air are 2.1 and 9.5 vol. %, respectively (Eckhoff,2005).*

4.2.2 Determination of probability of ignition

The discrepancy between the MIE value of 0.25 mJ claimed by Lewis and von Elbe (1961) and the value 0.46 mJ found by Moorhouse *et al.* (1974) called for a closer investigation of whether this could be due to different statistical treatment of the data. According to Moorhouse *et al.*, Lewis and von Elbe's MIE values referred to 1 % probability of ignition. It was therefore decided to perform a statistical analysis of the experimental data obtained for 5.5 and 5.2 vol. % propane in air.

The first test series was performed with 5.5 % vol. propane/air mixture, and 20 tests were done for each different spark energy levels by varying capacitors of values 14.0, 19.0, 23.0 and 28.6 pF. No ignition was observed with the 14.0 pF capacitor, or a spark energy of 0.33 ± 0.04 mJ. By increasing the value of the connected capacitor to 19.0 pF, the applied spark energy was increased to 0.41 ± 0.05 mJ, but still no ignition was observed. The same numbers of tests were performed with capacitors of value 23.0 pF (0.53 ± 0.06 mJ) and 28.6 pF (0.76 ± 0.06 mJ), obtaining ignition probabilities of 25 % and 100 %, respectively.

The second test series were done with 5.2 % vol. propane/air mixture. The results showed no significant difference in the probability of ignition for mixture concentration of 5.5 and 5.2 vol. %, even though it was expected that the mixture of 5.2 vol. % would be slightly more ignitable. Both mixture concentrations had an ignition probability of 25% when using the capacitor of value 23.0 pF. The spark energy level for 5.5 vol. % mixture was 0.53 ± 0.06 mJ and for 5.2 vol. % 0.49 ± 0.09 mJ. It is also important to emphasis that the probability of ignition is strongly dependent on the stability of the spark i.e. the voltage deposit in the spark.

In figures 4.3 and 4.4 the probabilities of ignition (y-axis) are plotted as function of the arithmetic mean spark energy values for each series of 20 tests and their standard deviations (x-axis). The ignition probabilities are calculated from equation 2.7 (P=m/n). A linear regression trend line is added with respect to the average values of ignition energy. The results suggest that the probability of ignition is a linear function of the spark energy, where the ignition probability of a mixture increases when higher spark energy is applied.

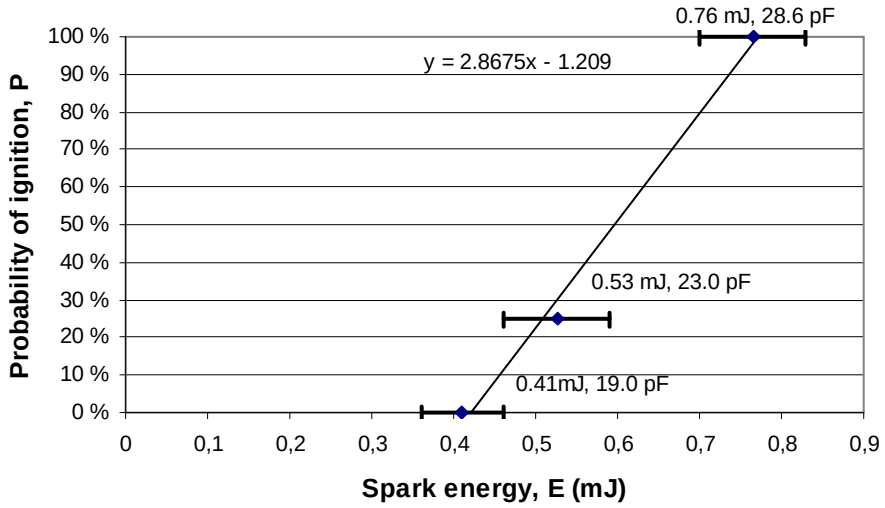

***Figure 4.3**: Probability of ignition for 5.5 vol. % propane/air. The average value of ignition energy and the values of the capacitors connected to the spark gap are noted in the diagram.*

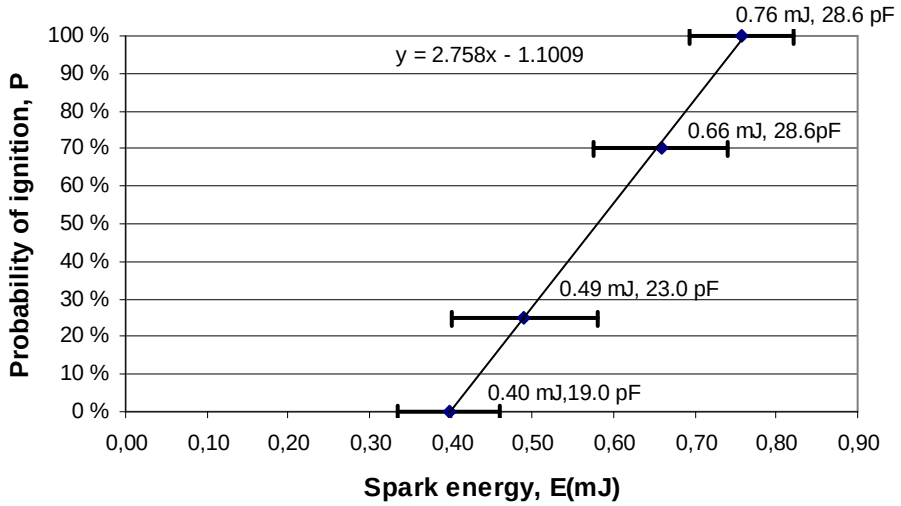

***Figure 4.4**: Probability of ignition for 5.2 vol. % propane/air. The average value of ignition energy and the values of the capacitors connected to the spark gap are also noted in the diagram.*

Ignition probability calculated by using logistic/binary regression

According to statistic literature, logistic regression is a convenient approach for modelling binary response and it is used extensively in the biological sciences, biomedical research, as well as in engineering.

The probability of ignition for 5.2 vol. % propane/air mixtures was calculated by using equation 2.8. The upper and lower limits for the 95% confidence envelope (UCL and LCL) were calculated by using equation 2.10, and the results are plotted in Figure 4.5 as a function of the spark energy.

The values of β_0, β_1, ρ and standard deviations of β_0 and β_1 in equation 2.8 and 2.10 can be found by using statistical tools SAS, PROC or SPSS. In the present work, SPSS (Statistical Package for the Social Sciences) was used. The variances σ_{00} and σ_{01} were calculated as the square of the standard deviations. Based on the data from 80 tests for 5.2 vol. % propane mixture, SPSS gave $\beta_1 = 33.070$ and $\beta_0 = -19.370$, $\rho = -0.995$ and standard deviations for β_0 and β_1 of 5.142 and 8.677, respectively.

$$P(E) = \frac{1}{1+e^{-\beta_0-\beta_1 E_i}} = \frac{1}{1+e^{19.370-33.070E_i}} \tag{2.8}$$

$$UCL/LCL = E \pm z_{\alpha/2}\sqrt{(\sigma_{00}+2E\sigma_{01}+E^2\sigma_{11})/\beta_1^2} \tag{2.10}$$

Where

$$\sigma_{01} = \rho\sqrt{\sigma_{00}\sigma_{11}} = -0.995\sqrt{5.142^2 8.677^2} = -44.394$$

and

$$UCL/LCL = E \pm 1.96\sqrt{(5.142^2 + 2E(-44.394) + E^2 8.677^2)/(33.070)^2}$$

Figure 4.5 shows the logistical probability distribution and the 95% confidence envelope for spark energy of 5.20 vol. % propane/air mixture. Probability of ignition, P (y-axis) is plotted as a function of spark energy, E (x-axis). The figure reveals the S-shaped function that approaches P = 1.0 as an asymptote. The original experimental data are also plotted in the diagram. For a given spark energy, E, the ignition probability, P(E) is unity for ignition and zero for no-ignition. Based on the data obtained in the present work, the most interesting ignition energy levels are in the range of 0.50-0.65 mJ, where ignition and no-ignition data overlap.

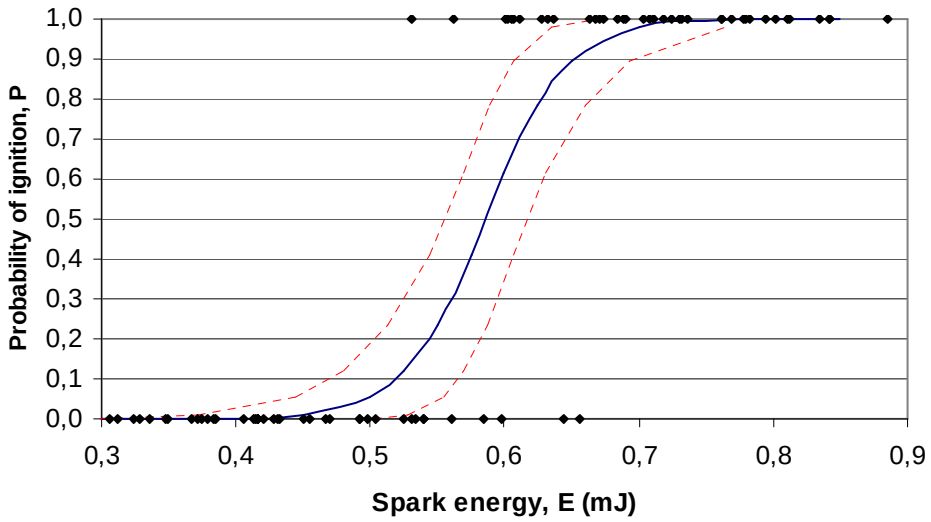

***Figure 4.5**: Logistical probability distribution and 95% confidence envelope for spark ignition data of 5.2 % vol. propane/air mixture. The original data are also plotted in the diagram. For given spark energies E, probability of ignition is 1 for " ignition" and 0 for " no-ignition".*

Logistic regression was also used to calculate the probability for the ignition of 5.2 vol. % mixture based on the 40 test data, where most energy levels for ignition and non-ignition overlap. The analysis gave β_1 = 27.743, β_0 = - 16.240, ρ = -0.996, and standard deviations for β_0 and β_1 of 5.334 and 9.046, respectively. The probability of ignition and the upper and lower critical limits were also calculated by using equation 2.8 and 2.10. Figure 4.6 shows that the S-shaped curve based on 80 tests is a little bit steeper than the one based on 40 tests, otherwise the two S-curves are quite similar. When the probability of ignition is in the range 40-60%, the two S-curves give practically the same calculated spark energy level.

Lewis and von Elbe used a probability of ignition of 1% and obtained a MIE value of order 0.25 mJ for 5.2 vol. % propane/air. By using linear and logistic regression methods, the corresponding energy levels based on the present data were calculated. The results are listed in Table 4.1. The calculated values of spark energy for probabilities of ignition of 1% and 50% indicated that the two probability calculation methods give almost the same results. According to the calculated data obtained by using logistic regression, for 1% probability of ignition, the spark energy is in the relatively wide range of 0.42 ± 0.11 mJ.

In the present study, it has not been possible to trace any statistical information in the work of Lewis and von Elbe. Therefore it is not clear which method Lewis and von Elbe did use to obtain the exact MIE value for propane/air of 0.25 mJ for a 1% probability of ignition. In particular, it is not known whether the value was obtained experimentally or via some mathematical model of ignition frequency as a function of spark energy.

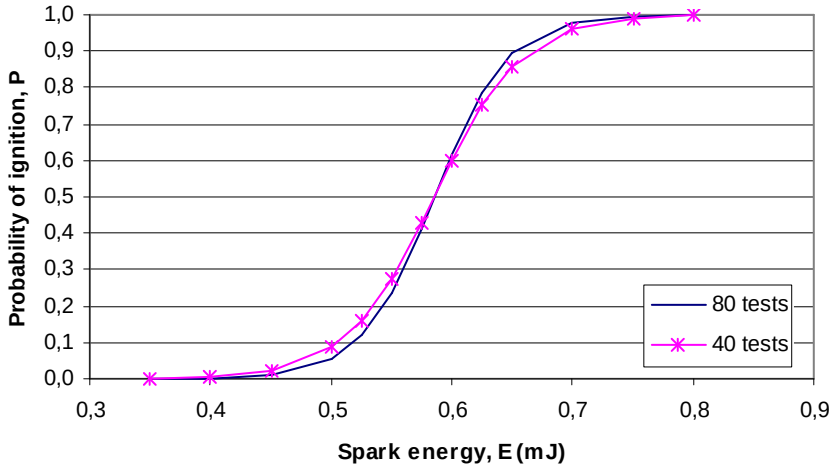

***Figure 4.6**: Logistic regression analyses of probability of ignition for 5.2 vol. % propane/air based on 40 and 80 tests.*

***Table 4.1**: Calculated spark energy levels, E, for 5.2 vol. % propane/air when the probability of ignition is 0.01 and 0.5 based on the experimental data obtained by using ASTM in the present work.*

	E calculated by linear regression	E calculated by logistic regression based on 80 tests	E calculated by logistic regression based on 40 tests
P = 0.01	0.40 ± 0.06 (mJ)	0.45 ± 0.08 (mJ)	0.42 ± 0.11 (mJ)
P = 0.50	0.58 ± 0.07 (mJ)	0.59 ± 0.03 (mJ)	0.59 ± 0.03 (mJ)

4.2 RESULTS OBTAINED WITH THE SYNCHRONIZED SPARK GENERATOR

Originally, the experimental work was supposed to cover the entire range of explosive propane concentrations in the same manner as for the ASTM method. However, due to the time required for developing the spark generator, there was only time for a limited number of tests. It was decided to confine all the tests to the most ignitable concentration, i.e. 5.2 vol. %. The aim was to find out if the new spark generator would give the same MIE as the ASTM.

Capacitors of values 2.0, 5.0, 3.3 and 10 pF were used to vary the spark energy. A few tests were also done when no explicit capacitor connected to the spark gap, i.e. when the only energy storage capacitance was the stray capacitance estimated to about 2.0 pF.

Resistor values of 39, 110 and 165 kΩ were introduced upstream of the spark gap to study the influence on the spark energy.

The peak voltage of the pulse over the spark gap was registered for every test, and the discharge voltage was calculated from equation 3.3 with the assumption that the spark occurred at the peak voltage of the pulse across the spark gap in all tests. Based on 50 successive tests, it was concluded that the voltage across the spark gap was in the range 9-12 kV.

However, due to the statistical nature of spark discharges, the spark does not always occur at the peak voltage. The duration of the additional energy supply following the first high-current pulse therefore varies from 1 to 3 µs, depending on the time when the spark occurs and the value of the connected resistor. Hence, the calculated additional energy might have been either under- or over-estimated in the present work.

Ideally a Labview program can be used to record the form and duration of the pulse for every test. In that way the discharge voltage and the duration of the additional energy for every successive spark triggering can be calculated more accurately. This may be the solution for future versions of the synchronized spark generator.

In the experimental work, most tests were done with a resistor of value 39 kΩ. When the value of the connected resistor R increases to 110 and 165 kΩ, the time constant (RC) is increased, causing a lower discharge voltage V_1. The time duration of the additional energy supply was set to 3µs in all tests.

The spark energy was calculated by using equation 3.2. The data for each of the 50 tests are given in Appendix C. The calculations show that the additional energy produced by the new synchronized spark generator is in the range of 0.06-0.25 mJ, which is significant lower than the value of about 1 mJ found with the original generator (Eckhoff *et al.* 2008).

Figure 4.7 provides a summary of the results obtained from 50 tests performed with the new synchronized spark generator. Due to the inevitable inaccuracy in the calculation of the spark energies, a precise conclusion cannot be drawn with respect to the MIE for propane/air produced by the new spark generator. However, the 50 data points do indicate a boundary between ignition and no-ignition in the order of 0.36 mJ for propane/air mixture of 5.2 vol. %. This value is lower than the MIE of 0.48 mJ, achieved by using the ASTM spark generator.

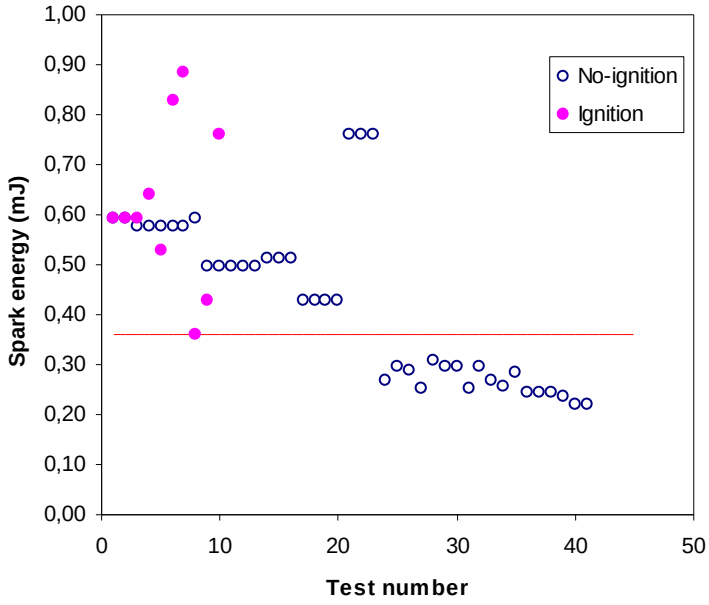

***Figure 4.7**: Experimental spark energy data of 5.2 vol. % propane/air mixtures achieved by using the improved synchronized spark generator of Randeberg et al. (2006).*

CHAPTER 5: CONCLUSIONS AND SUGGESTIONS FOR FURTHER WORK

5.1 CONCLUSIONS FROM APPLYING THE ASTM METHOD FOR MIE DETERMINATION

1. A study of the literature revealed a discrepancy between the classical MIE value for propane/air of 0.25 mJ reported by Lewis and von Elbe (1961), and the value of 0.46 mJ found by Moorhouse *et al.* (1974). According to the latter workers, Lewis and von Elbe defined their MIEs as the spark energy yielding an ignition probability of only 1 %. Moorhouse *et al.* adopted a pragmatic criterion for determining MIE, based on drawing the highest possible border line through their array of experimental ignition/no ignition points, below which there were no ignitions. The minimum value of this U-shaped border line was taken as the MIE.

2. In the present experimental investigation, using the pragmatic criterion suggested by Moorhouse *et al.* and a copy of ASTM's spark circuit, the MIE for propane in air was found to be 0.48 mJ. This is in very close agreement with the value found by Moorhouse *et al.*, but twice the value reported by Lewis and von Elbe.

3. The experimental data also showed that the gap of 2.0 mm between the flanged electrodes equals the quenching distance for a propane/air mixture of around 4.0 vol. % on the fuel lean side, which is in good agreement with the results of Lewis and von Elbe. On the other hand, it was not possible to define any specific propane concentration on the fuel rich side for which the quenching distance was 2.0 mm. Lewis and von Elbe claimed that on the fuel rich side 2.0 mm would be the quenching distance for 6.0 vol. % propane in air.

4. In the present investigation, the most easily ignitable propane concentration was about 5.2 vol. %, but 5.5 vol. % gave practically identical result.

5. The probability of ignition increases with spark energy. By applying a logistic regression analysis to the data obtained for 5.2 vol. % and 5.5 vol. % respectively, the spark energies giving 1% and 50 % probability of ignition were calculated. The spark energy giving 50 % probability of ignition was 0.59 ± 0.03 (mJ), whereas that giving 1 % probability was 0.42 ± 0.11 (mJ). The calculated MIE value for 1 % probability of ignition of 0.42 mJ is significantly higher than the value of 0.25 mJ of Lewis and von Elbe.

5.2 CONCLUSION FROM APPLYING THE SYNCHRONIZED SPARK GENERATOR FOR MIE DETERMINATION

A modified version of the synchronized spark generator described by Randeberg *et al.* (2006) was constructed. However, due to considerable challenges during this work, there was only time left for a limited series of ignition experiments with propane/air, using a preliminary prototype of the generator. The data obtained indicate a border line between ignition and no-ignition of about 0.36 mJ for mixture of 5.2 vol. % propane in air. So far, the residual energy produced by the new synchronized spark generator is significantly lower than for the original one, typically 0.25 mJ as opposed to the original 1 mJ.

5.3 SUGGESTIONS FOR FURTHER WORK FOR THE SYNCHRONIZED SPARK GENERATOR

During the experimental test program, there were many non-successful attempts at triggering the spark. The high-voltage transformer T2 should therefore have more secondary windings to achieve voltages higher than 12 kV, and hence more reliable spark triggering. It should also be considered to use needle shaped electrodes tips to lower the breakdown voltage.

All the pulse generators (P1-P4 in Figure 3.2) can in principle be replaced by a crystal oscillator to achieve a more precise time reference. In the present work, one pulse is used to trigger another, and the time reference of the pulse generators are based on an analogue RC-system. Limited precision with respect to timing may affect the shape and amplitude of the pulse across the spark gap and cause inaccuracy in the energy calculation.

A high-voltage probe with a scale-down ratio of 100:1 or 200:1 should replace the high-voltage probed with a scale-down of 1000:1 used in the present work. This would simplify the process of amplifying the tail of the pulse to recover its original shape and amplitude, and eliminate some of the inaccuracies in the present system.

Calculations suggest that the residual energy may decrease from about 0.25 mJ to less than 0.1 mJ by increasing the value of the resistor connected in series with the spark gap from 39 kΩ to 110-165 kΩ. This should be explored further in the future studies.

A Labview program can be connected to the oscilloscope that registers the spark occurrence for every test. The duration of the residual pulse i.e. the duration of the additional energy can thereby be estimated and the calculated spark energy will be more accurate.

It is recommended that a complete series of ignition tests for propane/air be undertaken with the new version of the modified synchronized spark generator.

LIST OF REFERENCES

ASTM (2007): *Standard test method for minimum ignition energy and quenching distance in gaseous mixtures.* Designation E 582-07. ASTM Int.

Babrauskas, V. (2003*): Ignition Handbook*, Published by Fire Science Publishers, A division of Fire Science and Technology Inc., Issaquad, WA 98027, USA.

Blanc V. M., Guest P. G., von Elbe G and Lewis B. (1947): *J. Chem. Phys. 15, 798*; "Third Symposium on Combustion and Flame and Explosion Phenomena", pp. 363, William & Wilkins, Baltimore, 1949.

Calcote H. F., Gregory C.A., Barnett, and Gilmer (1952): *Spark ignition, Effect of Molecular Structure*. Industrial and engineering chemistry 44 (1952).

Cheng, D. Y (1967): *the name of the article was not possible to trace in this present work*, Combustion Flame, Vol. 11, pp. 517.

Crowl, D. (2003): *Understanding explosions*, American Institute of Chemical Engineers.

Eckhoff, R. K. (1970): *The energy required for the initiation of explosions in dust clouds by electric sparks*, M.Phil. Thesis, University of London.

Eckhoff, R. K. (2003): *Dust Explosion in Process industries*, 3rd edition, Gulf Professional Publishing. ISBN 0-7506-7602-7

Eckhoff, R. K. (2005): *Explosion Hazards in process industries*, 1st edition, Houston, Texas, Gulf Publishing Company. ISBN 0-9765113-4-7

Eckhoff R. K., Olsen W. and Kleppa O. (2008*): Influence of spark discharge duration on the minimum ignition energy of premixed propane/air*, Proc. 7th International Symposium on Hazards, Prevention and Mitigation of Industrial Explosions. St Petersburg, Russia, July 2008. Published by Semenov Institute of Chemical Physics.

Glor, M. (1984): *Condition for the appearance of discharges during the gravitational compaction of powders*, J. Electrostatic 15, pp. 223 – 235.

Guest, P. G. (1944*): U.S. Bur. Mines, Rept. Invest*. 3753.

Kleppa O. (2008): *Minimum ignition energy of propane/air*, Master thesis (in Norwegian) submitted to University of Bergen, Norway.

Kono M., Kumagai and Sakai T. (1976): *The optimum condition for ignition of gases by composite sparks*, Proc. 16th Symposium (international) on combustion, pp. 757-766, The Combustion Institute, Pittsburgh, USA.

Kono, M. and Hatori, K. (1985): *Ignition of low flow velocity mixture by short duration sparks*, pp. 500 – 503 in GD85 – 8th Intl. Conf. on Gas Discharges & Their Applications, Leeds Univ. Press, Leeds.

Kono M., Isshii K., Tsukamoto T. and Ujiie Y. (1992): *Analysis of ignition mechanism of combustible mixtures by composite sparks,* Combustion and Flame, Vol. 91, pp. 153-164 (1992).

Ko, Y., Anderson R.W. and Arpaci V.S (1991): *Spark ignition of propane/air mixtures near the minimum ignition energy*: Part I. An experimental study, Combustion and flame, Vol. 83, pp. 75-87.

Kravchenko, V.S, Serov (1980): *Chapter 3. Ignition of explosive mixtures by electric discharges*, *The relationship between the ignition energy and the duration of its release,* Health and Safety Executive Translation Service, Transl. No. 8900, April 1980.

Kravnchenko, V.S, and Bondar, V.A (1982): *Explosion safety of electrical discharges and frictional sparks*, Part1, Chapter 1, pp. 5-71, Health and Safety Executive Translation Service, Transl. No 8346, March 1982.

Lee T., Jain V. and Kozola S. (2001): *Measurements of minimum ignition energy by using laser sparks for hydrocarbons fuels in air: propane, dodecane and jet-A fuel.* Combustion and Flame, volume 125, Issue 4, June 2001, pp. 1320-1328.

Lewis, B. and Elbe, G. von (1961): *Combustion, flames and explosions of gases*, 2nd edition, Academic Press, Florida and London.

Litchfield, E.L, Hay M.H., Kubala T.A and Monroe J.S. (1967): *Minimum ignition energy and quenching distance in gaseous mixtures*, U.S Bureau of Mines Report of Investigation no. 7009.

Lüttgens and Glor (1989): *Understanding and controlling static electricity*, Leverkusen: Expert Verlag.

Magison E.C. (1988): *Electrical Instruments in Hazardous Locations*, 4th edition, ISA- The Instrumentation, Systems and Automation Society.

Maly R. and Vogel M. (1978): *Initiation and propagation of flame fronts in lean CH4-air mixtures by the three modes of ignition spark*, in Proc. of 17th Symp. (Internat.) on Combustion: The Combustion Institute, pp. 821-831.

Moorhouse, J., William, A. and Maddison, T.E (1974): *An investigation of the minimum ignition energies of some C1 to C7 hydrocarbons*. Combustion and Flame, vol. 23, pp. 203-213.

Moffett S. P., Bhanderi S. G., Shepherd J. E., Kwon E. (2007): *Investigation of Statistical Nature of Spark Ignition*, Paper # 07F-42, 2007 Fall Meeting of the Western States Section of the Combustion Institute, Sandia National Laboratories, Livermore, CA.

Parker, S.J (1985): *Electric spark ignition of gases and dusts*, PhD thesis, the city university, London, UK.

Randeberg E. (2006): *Electric spark ignition of sensitive dust clouds in the sub 1mJ range*, Dr. scient. Thesis, Department of Physics and Technology, University of Bergen, Norway.

Randeberg E., Olsen W. and Eckhoff R.K (2006): *A new method for generation of synchronised capacitive sparks of low energy*, Journal of Electrostatics, 64, pp. 263-272.

Randeberg, E. and Eckhoff, R.K (2007): *Measurement of minimum ignition energies of dust clouds in the < 1 mJ region*, J. Hazardous Materials, Vol. 140, pp. 237-244.

Strid K.G (1973*): Experimental Techniques for the determination of ignition energy.* Oxidation and Combustion Reviews, Vol. 6, pp. 1-46. Elsevier Scientific Publishing Company, Amsterdam – Printed in The Netherlands.

Trek (2002): *AC-feedback electrostatic voltmeter measurements, Trek Application Note No. 3004*. Available at www.trekinc.com/library/Tech_Notes/asp

APPENDIX A: GENERAL THEORY

A.1 Electrostatic discharges

Babrauskas (2003) divides electrostatic discharges into 6 categories:

1) Spark discharge

According to Lüttgens and Glor (1989) the term spark can be defined as a disruptive discharge through a single ionization channel that bridges the gap between two conductive electrodes. Electrical sparks (or break sparks) are formed by the breaking of low-voltage high-current circuits. Electrostatic sparks are high-voltage low current phenomenon occurring when the electric field is sufficiently high to cause electrical breakdown of the prevailing/existing gas between the two electrodes.

For a gap distance d, the voltage U required for achieving breakdown of a uniform electric field is 3d, where U is in megavolts and d in meters. A normal electric spark discharge occurs through the air separating two electrodes when electric field reaches a value of approximately 3 MVm^{-1}. For a spark to be incentive, the gap distance normally must be equal or greater than the quenching distance. So for a typical gap distance of 2 mm, the breakdown voltage required is in the order of 6 kV. In a spark an energy amount up to 1000 mJ can be delivered.

According to Paschen's law, the breakdown voltage of a uniform field is a function of pressure and gap length for a given gas and electrode material. For non uniform field, the breakdown voltage for short gaps with thin electrodes is proportional to the square root of gap length.

2) Corona discharge (point discharge)

Corona discharge is a slow, diffuse discharge that originates at a metallic electrode and branches out in a diffuse manner into space or towards poorly conducting surfaces.

Corona discharge occurs when a conducting (needle like) electrode tip with radius less than 5 mm approaches a charged non-conductor.

This type of discharge occurs as a continuous charge leakage. Unlike a spark or an arc, a corona discharge does not create a hot, conducting plasma channel. A corona discharge

can occur in the presence of the second electrode, but is still considered as a one electrode discharge since the discharge does not actually reach the second electrode. A minimum voltage of about 2-6 kV is needed for a corona discharge to occur. The energy from corona discharge will be about 0.01 mJ.

3) Brush discharge

Brush discharge is also a one electrode discharge and similar to corona discharge. But the conducting electrode has radius of about 5-50 mm.

A minimum potential difference of 20-25 kV is needed for a brush discharge to occur. It is estimated that the energy from brush discharge will not be greater than 4 mJ. In addition, most of the energy released during a brush discharge does not contribute to incendivity, because the energy is not just localized at the place where a flame kernel is formed. Thus only 10% of the energy released is actually effective towards ignition.

For brush discharge to ignite a flammable gas mixture, it is necessary that the insulator /conductor gap over which the discharge occurs be greater than 20-30 mm.

4) Propagating brush discharge (Litchenberg discharge)

A propagating brush discharge can ignite most flammable mixtures, including dust clouds. The discharge can occur in two ways:

a) A grounded electrode is brought near the charged insulator surface.

b) A dielectric breakdown of an insulating layer, resulting a local puncture.

A propagating discharge is capable of discharging nearly all of the charge stored in the double layer. A propagating brush discharge does not occur if the thickness of the insulating is greater than 8-10 mm, but it also is less likely to occur with very thin insulating layers. For the charge build-up to be successful, the insulating layer has to have a high dielectric strength.

Energy in the order of 1000 mJ can be delivered in propagating brush discharge.

5) Powder heap discharge (cone discharge or bulking discharge)

It occurs along the exposed surface of the powder. According to Babrauskas (2003), Glor (1984)'s computation showed that a minimum particle size of ca. 0.1 mm is needed for powder heap discharge to occur. But most actual incidents have involved polymeric resin particles in the 1-10 mm range. Glor also concluded that discharges as large as 1000 mJ may be anticipated for large particles flowing into a large silo.

For 3 mm particles a minimum product feed rate of about 3000-5000 kg/h is needed for powder heap discharge to occur. This feed rate rises to 25 000-30 000 kg/h for 0.8 mm particles. Powders having a resistivity of less than 10^{10} Ω-m are conservatively judged to not be susceptible to explosions from powder heap discharges. Powders which have caused explosions have had resistivity greater than 10^{12} Ω-m.

6) Lightning-like discharge

Lightning in the atmosphere can occur when water droplets and ice particles are charged to very high potentials. Since particles in dust clouds will also pick up an electric charge, lightning like discharges have been observed to occur in the dust clouds formed during volcanic eruptions. According to the experiments voltage values greater than 300-500 kV/m are needed for lightning discharge to occur. However the events caused by this type of discharge are expected to be very rare because normal transport of dusts does not lead to high electrical charging.

A.2 Properties of spark discharges

Both ignition and the subsequent flame propagation are strongly influenced by the discharge mode and the geometry of the plasma volume. The total energy involved plays only a minor role. The study of Maly and Vogel (1978) provides a details explanation of the spark discharge process, divided in three main phases which are *breakdown, arc* and *glow phase*. Figure A.1 shows typical gap voltage and current as function of time during a spark discharge.

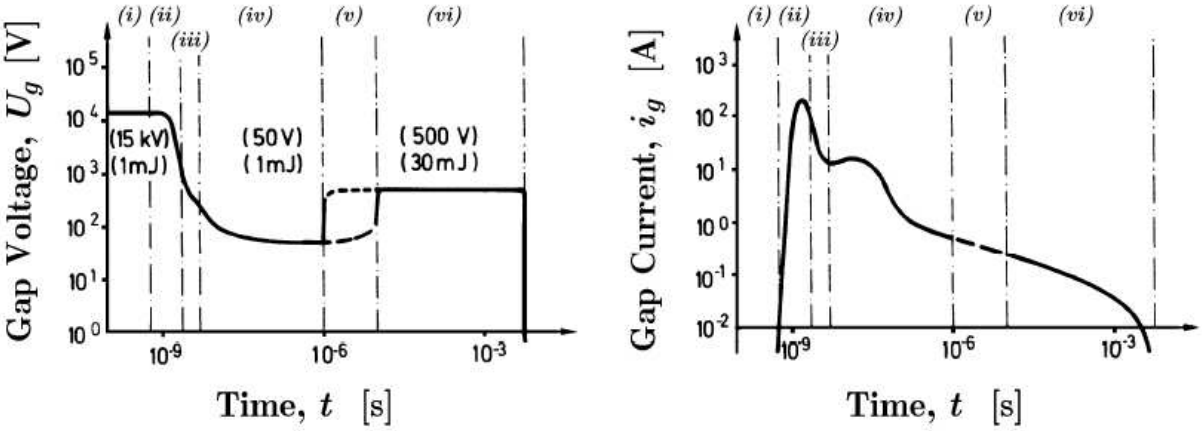

Figure A.1*: schematic diagram of voltage and current vs. time in a spark discharge of a typical spark ignition system. The six discharge phases are: i) pre-discharge, ii) breakdown, iii) breakdown/arc transition, iv) arc, v) arc/glow transition, and vi) glow. From Maly and Vogel (1978)*

The details of electric spark ignition are complex and involve an interaction of physics and chemistry effects. The six discharge phases can be shortly described as:

i) **Pre-breakdown phase**: When the spark pulse is applied, increasing the electric field, free primary electrons are accelerated towards the anode. By electron collisions, these electrons can ionize neutral gas molecules, producing additional secondary electrons and ions. Not every electron collision leads to ionization. But some of the atoms in the gas become excited by collisions with electrons of lower energies than ionization energy. Those excited atoms produce UV radiation that can ionize other atoms (photo-ionization) when they recover to their original state. In this way, the origin of the electron avalanches can move closer to the cathode and the ionization would occur closer to cathode. Eventually, positive ions are generated sufficiently close to the cathode to be accelerated towards it.

   When the kinetic energy of the ions exceeds twice the work function of the electrode material, electrons may be liberated from the cathode surface, triggering a positive feedback loop. The number of electrons and ions increase rapidly (avalanche) and conducting channel are formed. The pre-breakdown phase lasts as the ionizing process produce fewer electrons than required for rendering the discharge self-sustained. The duration is determined by the rate of rise of the gap voltage.

ii) **Breakdown phase**: when enough feedback electrons are produced, the discharge current increases significantly from ~10 mA to ~200 A during ~1-10 ns. At the same time, the voltage drops dramatically from ~10 kV to ~100 V. The impedance of the discharge circuit is the only factor limiting the current during the breakdown phase. The temperature and pressure rise rapidly (to ~ 60 000 K and ~200 bar), resulting in the emission of a shock wave. About 30% of the energy carried by the shock wave heats the surrounding gas within a very small sphere (diameter ~1mm). Due to the short duration, more than 80 % of the energy discharged in breakdown phase is transferred to the plasma.

Figure A.2 shows the gap current increases with decreasing gap resistance. Eckhoff (2003) analyzed a number of studies and concluded an empirical relation:
$R = 40\ L_s I_s^{-1.46}$ where R = gap resistance (ohm), L_s = spark gap (mm) and I_s = current (A). The studies were based capacitive discharge, and it's also important to notice that the relation only valid for discharge currents of 1.0 mA to 10 A.

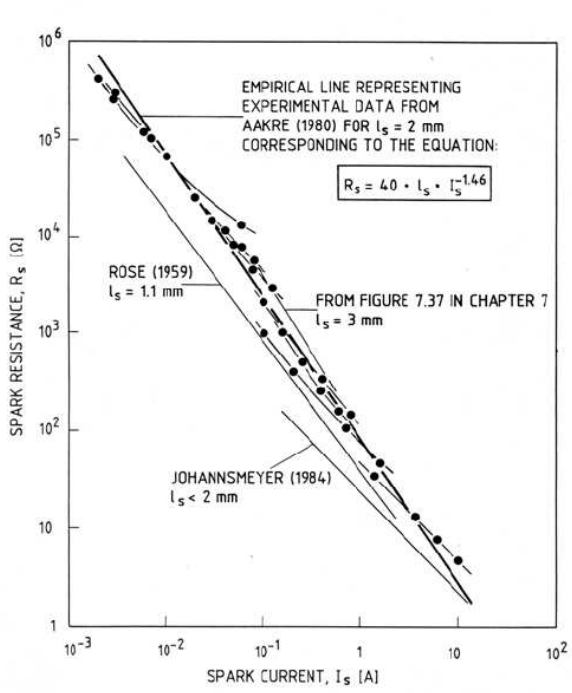

***Figure A.2**: Spark gap resistance R_s as a function of spark current I_s for capacitive spark discharges across a 2 mm spark gap in air at normal pressure and temperature (Data from Aakre, 1980). Comparison with data for shorter gaps from Rose (1959) and Johannsmeyer (1984), and for a 3 mm gap from Figure 7.37 from Eckhoff (2003), L_s is the length of the spark gap in mm. The Figure is taken from Eckhoff (2003).*

iii) **Breakdown/Arc transition region**: prolonged duration of high current flow leads to thermionic emission from hot cathodes, indicating the end of breakdown phase and start of arc regime. Both the gap voltage and current decrease rapidly.

iv) **Arc phase**: Electrons emitted from the hot cathode spots (pools of melted electrode material of 10-40 µm in diameter) are needed for the arc can be sustained. The gap voltage is very low (~50 V). The current varies from 0.5 mA to several kA, depends on the impedance of the external circuit. The equilibrium kernel gas temperature is only about 6000 K because the continuous energy losses to the electrodes. The energy transfer efficiency of the arc phase is up to 50%.

v) **Arc/Glow transition**: the glow phase begins when the cathode cools down. At currents of 100-200 mA, the discharge tends to oscillate between arc and glow. The discharge can be forced to glow by limiting the current.

vi) **Glow phase**: feedback electrons are liberated from the cathode by the ion impact. The gap current drops to less than 200 mA. The gap voltage in this phase is very low but constant at a value of about 500 V. Typical temperature of the equilibrium kernel gas is about 3000 K, with less dissociation and only about 0.01% ionized molecules. Glow discharge lasts for more than 1 ms.

Energy is transferred to the plasma very inefficiently because almost 70% of the supplied energy is lost to the electrodes.

Any spark ignition system includes different combinations of the breakdown, arc and glow discharge modes with varying energy and discharge durations. Capacitive discharge circuits (low impedance) favour arc discharge, whereas discharge circuits with series resistance or inductance favour glow discharge. The energy balances for the main three discharge phases are summarised in Table A.1.

Table A.1*: Energy balance for the three discharge phases: breakdown, arc and glow.*

	Breakdown (%)	Arc discharge (%)	Glow discharge (%)
Radiation loss	< 1	5	< 1
Heat conduction via electrodes	5	45	70
Total losses	6	50	70
Total plasma	94	50	30

A.3 The work of Kono *et al.*

By using a set of partial differential equations on two-dimensional cylindrical coordinates Kono et al. (1992) simulated flame kernel development produced in composite sparks. The flame kernel assumed to be symmetric and the computational region is 2x2 mm. The initial temperature and pressure of the quiescent mixture is 300 K and 0.1 MPa except within the spark channel. The mixture used in the simulation was stoichiometric propane/air

For the simplicity of the model, some assumptions were made. One of the assumptions was to neglect natural convection, heat transfer by radiation, and ionic wind effect. The boundary conditions are as follows: in Figure A.3 for (1) and (2) the velocities for r and x axis are zero. The gradients of all variables are zero for both boundaries. For (3) and (4), the gradients of all variables are zero. For (5) and (6), the surface of the spark electrode, no slip condition and heat transfer from the flame kernel to the spark electrode are assumed.

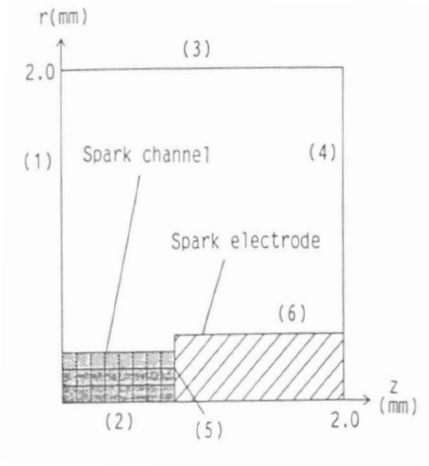

Figure A.3*: Region of simulation, notation of initial and boundary conditions.*

The flame kernel shape/development is governed by the gas flow pattern generated by the spark discharge. The simulation showed the effects of spark gap, spark electrodes' diameters and shapes on flow pattern i.e. flame kernel structure.

Figure A.4 and A.5 show the difference in the flame kernel structure when the spark gap was varying from 1 to 2 mm. In Figure A.4, due to the gas movements near the tip ends of the spark electrodes the flame kernel is divided into two parts: one is the ring of the torus and other exists in the spark gap. In Figure A.5, the gap distance here is 2 mm. As it could be seen, the flame kernel is not divided and has a torus shape. A distinctive difference in the flame kernel in Figure A.4 and A.6 can also be notice due to the effect of different thickness of the electrodes.

The existence of optimum spark durations was also reconfirmed in this study. Spark durations affects the flow patterns and the shape of flame kernel. Normally the shape of the flame kernel is elliptical shape at first, becomes a torus and afterwards changes into more or less spherical. Figure A.7, the spark duration is 10 µs, compared with Figure A.4, the spark duration was 2 µs, the flame kernel was still ellipsoid at 100 µs and the high-temp region was located at the gap centre. The strength of the shock wave and the velocity of the inward flow decreased for long duration spark under the same spark energy condition. Consequently the flame kernel did not become a torus and remained near the spark gap.

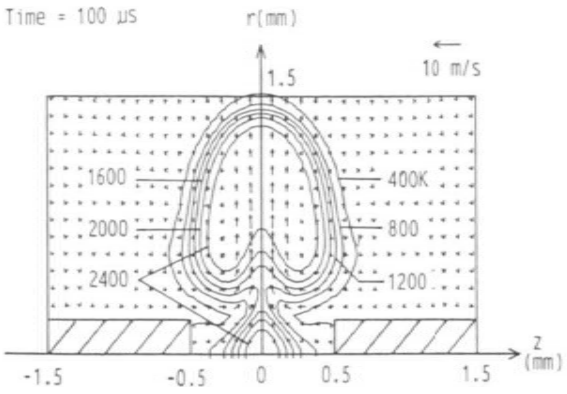

***Figure A.4**: Temperature and velocity distributions. Spark gap width: 1.0 mm; spark electrode: 0.4 in diameter.*

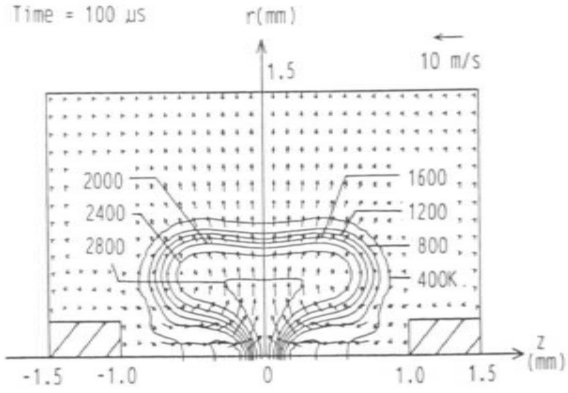

***Figure A.5**: Temperature and velocity distributions. Spark gap width: 2.0 mm; spark electrode: 0.4 in diameter.*

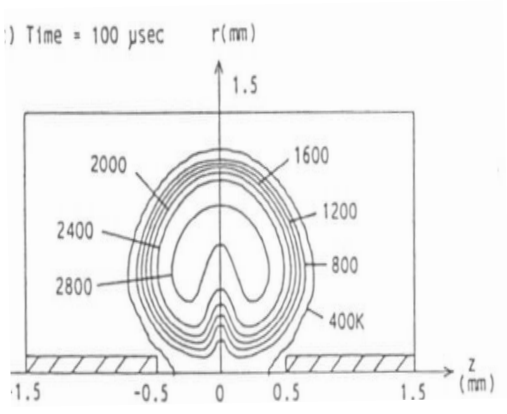

***Figure A.6**: Temperature and velocity distributions. Spark gap width: 1.0 mm; spark electrode: 0.2 mm in diameter. Spark duration: 2µs*

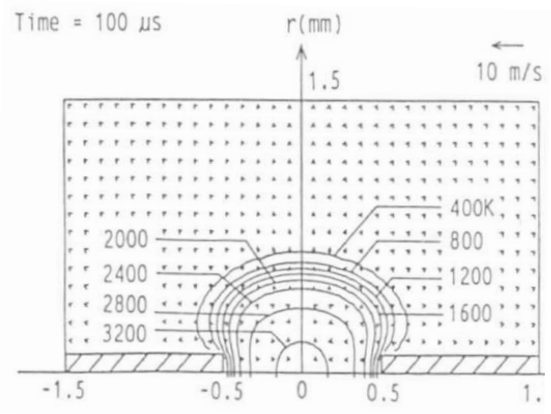

***Figure A.7**: Temperature and velocity distributions. Spark width 1.0 mm; spark electrode: 0.4 mm in diameter; Spark duration: 10 µs.*

Figure A.8 shows how the electrode tips affect the flow pattern when the spark gap is 1 mm. For the same test condition (the same electrode diameter and 1mm spark gap), in opposed to electrode tip of half cone angle of 45 degrees (a), half cone angles of 90 degrees (b) Both calculation and simulation show electrode tip of half cone angle of 45 degree causes less heat loss and is capable to cause a successful ignition.

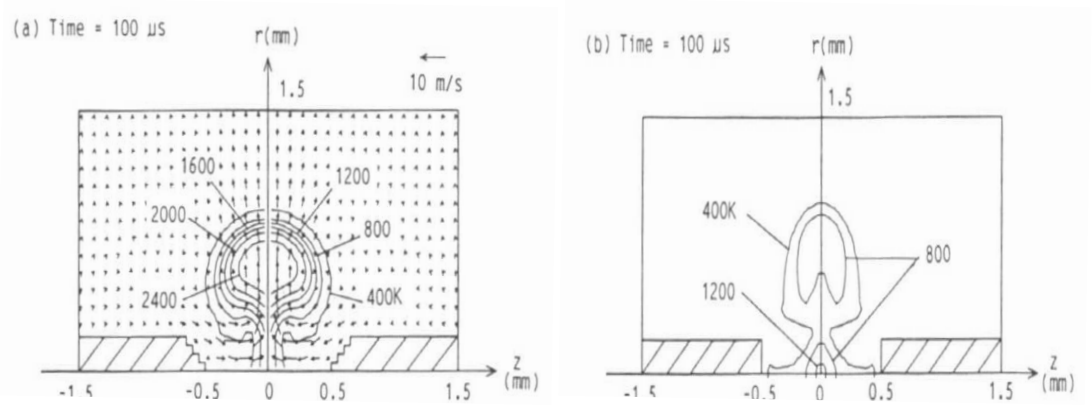

Figure A.8*: Temperature and velocity distribution. Spark gap width: 1.0 mm: spark electrode: 0.4 mm in diameter.*

The amount of heat loss to the spark electrode is affected by spark electrode configuration. The calculations in Figure A.9 show effects of electrode diameter and gap width on the heat loss. When the gap distance is 1.0 mm, a large amount of hot gas is captured in the spark gap. The recirculation flow moves the captured gas toward the spark electrode tip and contributes to the increment of the heat loss. The heat loss increases with electrode diameter. In the case of 3.0 mm gap width, the flame kernel is formed away from the spark electrode, so the heat loss in the early stage (less than about 10 μs) is independent of the electrode diameter.

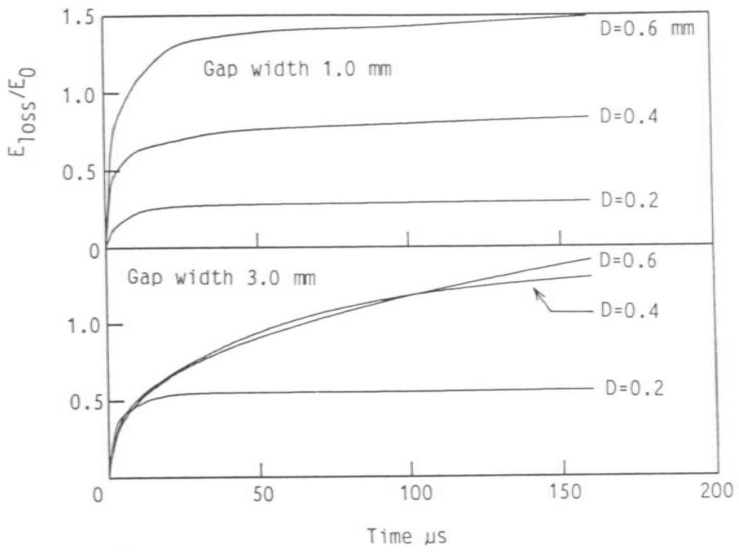

Figure A.9*: Ratio of heat loss to spark electrode surfaces (E_{loss}) to spark energy (E_0). D: diameter of spark electrode*.

APPENDIX B: APPARATUSES

B.1 Calibration results for electrostatic voltmeter and high-voltage supply

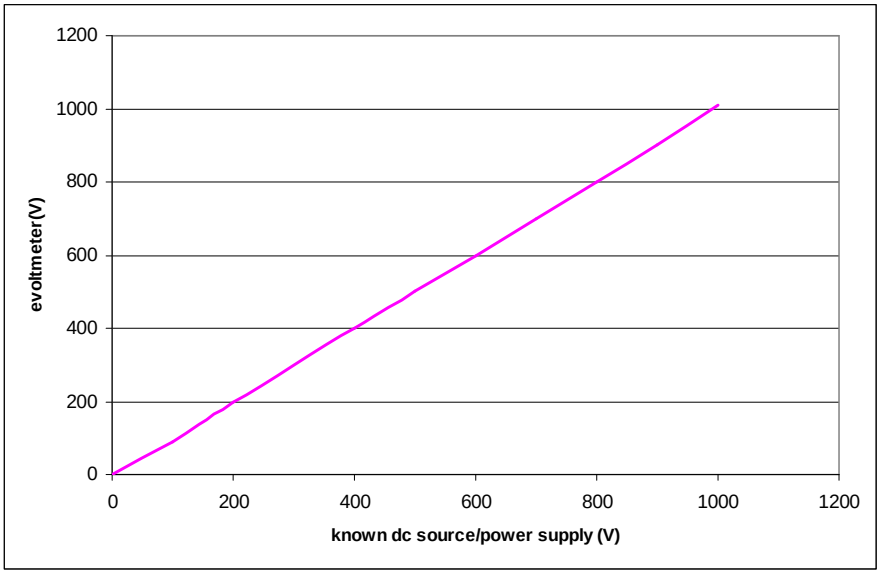

***Figure B.1**: The electrostatic voltmeter calibrated against a known dc power supplier. The graph shows a linear function with no offset error of these two apparatuses, indicating the voltmeter is giving correct reading voltage-values.*

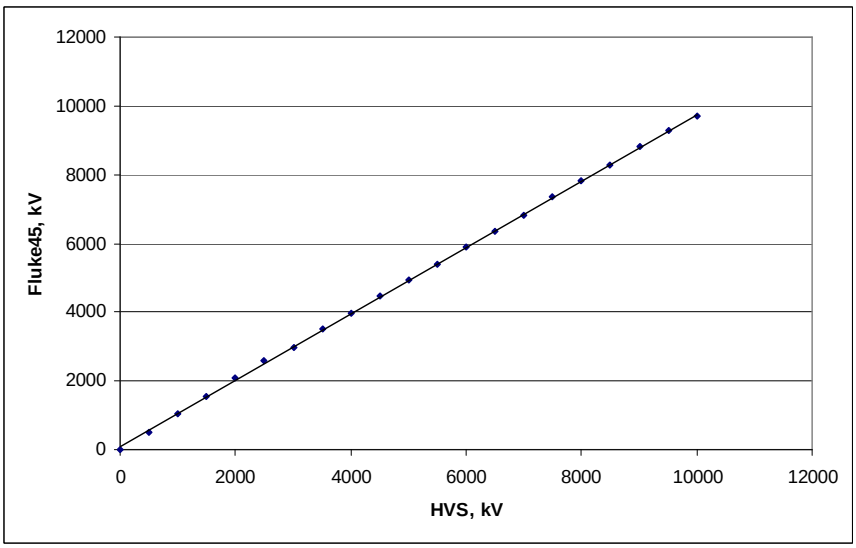

***Figure B.2**: High voltage supplier calibrated against a voltmeter, Fluke45. The results show the HVS is still applicable, delivering high voltage of value up to 10 000 kV.*

B.2 Gas mixing system for propane/air

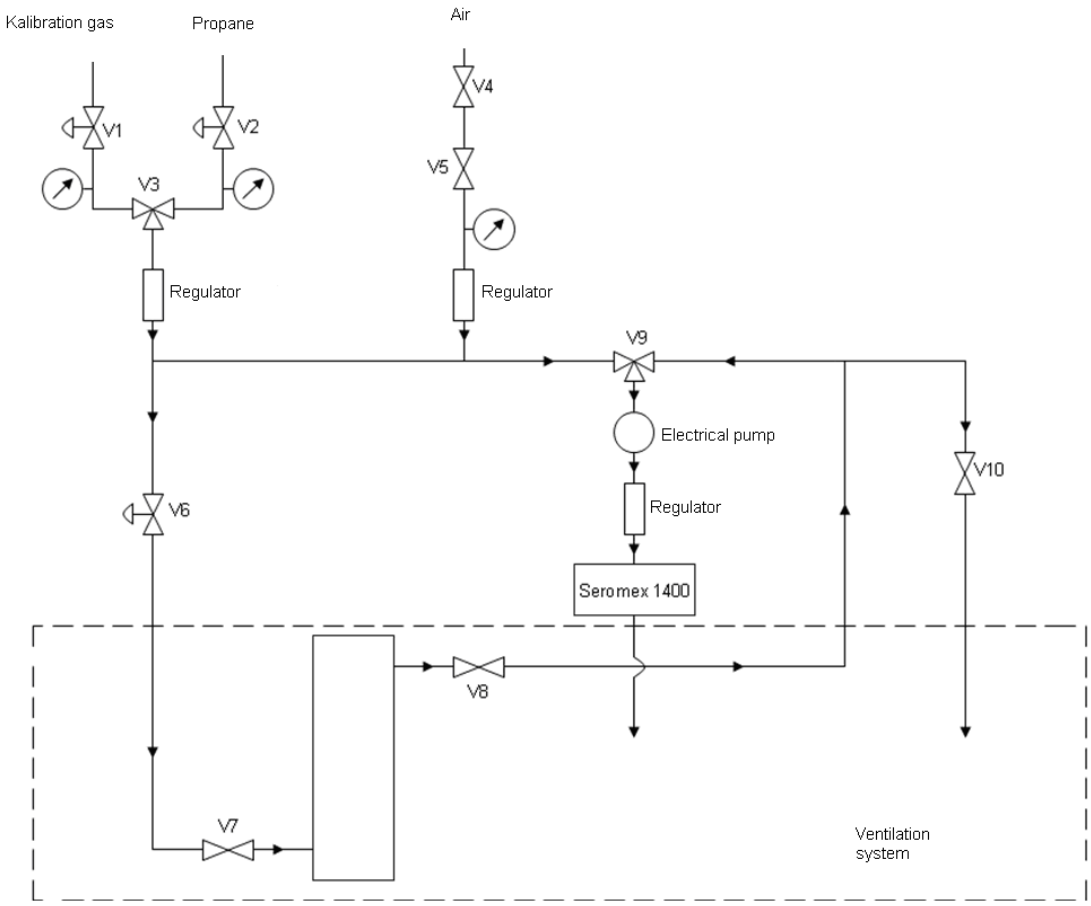

***Figure B.3**: Diagram of the gas mixing system. The figure is modified from Kleppa (2008)*

Air and propane gas enter the system through 2 main entrances. Compressed air enters the system with a pressure of 0.5 bars. The pressure is adjusted by using pressure reduction valve, V5. Propane gas or calibrating gas, selected by using valve 3, V3, enters the system with a pressure of about 10 psi. The amount of gas and air entering the system can be adjusted by using the flow regulators.

The function of valve 6, V6, is to allow the gas mixture flow to enter the explosion vessel. When the desired concentration is achieved, by closing valve nr 7 and 8, V7 and V8, the gas mixture in the explosion vessel is captured, ready to be tested. These two valves are connected/installed to the explosion vessel.

By using valve 9, V9, measurement of the concentration of the gas mixture before or after it enters the explosion vessel can be selected.

The concentration of the gas mixture is measured by Servomex 1410 B, infrared analyser. The gas mixture enters the gas analyser with a flow rate of around 500 ml/min after it has passed through an electrical pump and a flow regulator.

The gas mixture flows through valve 10, V10, before it releases to the vent. By using this valve allows the gas mixture flow can be returned to the system or released to the vent.

B.3 Servomex 1100A oxygen analyser

Because of the paramagnetic susceptibility, oxygen molecules are attracted by a magnetic field more than any molecules of other common gases. The 1100A oxygen analyser measures the paramagnetic susceptibility of the sample gas by means of a magneto-dynamic type measuring cell.

Servomex 1100 oxygen analyser contains two main units, a transducer and a control unit. The Transducer unit has three basic functional units.

1) Measuring cell
2) Heaters and temperature sensor
3) Pressure compensation (optional)

The Control unit has seven basic functional blocks:

1) Amplifier Board
2) Analogue to Digital Converter
3) Microprocessor Board
4) Isolated Current Output Board
5) Keypad
6) Display Board
7) Power supply Unit

For more details about the units mentioned above refers to the instruction manuals of Servomex 1100A.

After switching on, the analyser should be left for 12 hours for the temperature to stabilise before accurate measurements are made. The display shows the oxygen concentration with two decimal places.

The normal cell temperature is about 60° C. The cell temperature can be checked by pressing DISPLAY 17 on the keypad. The sample pressure should be within the range 0.3 to 20 psig (2 to 140 kPa).

Before performing the calibration, it is necessary to enter the oxygen content of the calibrating gases into the analyser. Once the oxygen contents have been stored and do not have to be re-entered unless the gases are changed or the microprocessor memory is lost because of battery failure. Zero gas calibration was done weekly and span-calibration daily.

To enter the zero gas oxygen content:

1) Enter the password by pressing 4 5 6 and then Enter button on the keypad.
2) Press SET GAS ZERO(7) 0 . 0 0 ENTER

The display should show 0.00 97

To enter the span gas oxygen content:

1) Enter the password by pressing 4 5 6 and then Enter button on the keypad.
2) Press SET GAS SPAN(8) 2 0 . 9 5 ENTER

The display should show 20.95 98

Zero calibration

Nitrogen gas is used as zero gas.

1) Introduce the zero gas into the analyser at a flow rate of about 200 ml/min and allow the oxygen reading to stabilize.
2) Check that the mechanical zero is within the tolerances by pressing Display 1 4 on the keypad. This should be within ±2%. If it is outside these limits the mechanical zero needs adjusting. Refer to section 4.3 in the introduction manuals.
3) Enter the password by pressing 4 5 6 and then Enter button on the keypad.
4) The zero calibration is done by pressing: SET, CAL, ZERO(7), ENTER

The display should show 0.01 77 for a successful zero calibration. Other values indicate an error and the zero calibration has not been done. See Table 3.1 page 3.16 in the instruction manual for a listing of manual calibration error messages.

Span calibration

A span calibration should only be performed until a successful zero calibration has been done. Air is used as a span gas. The span calibration is performed by:

1) Introduce span gas into the analyser at a flow rate about 200 ml/min and allow the oxygen reading to stabilise.
2) Enter the password by pressing 4 5 6 and then Enter button on the keypad.
3) The span calibration is done by pressing: SET, CAL, SPAN (8), ENTER

The display should show 0.01 78 for a successful span calibration. Other values indicate an error and the span calibration has not been done. See Table 3.1 for a listing of manual calibration error messages.

It is recommended that the span gas limits should be 25% of the oxygen content of the span gas being used. For air (21% oxygen) the tolerance is 5%. For more details about the operation refers to chapter 3 in the introduction manuals of Servomex 1100A.

The analyser has also alarm functions for oxygen levels, calibrations, cell-temperature and flow rate. For the details about the alarm functions and setting refer to chapter 3.8 in the instruction manual.

B.4 Servomex 1410, the gas analyser

The gas analyzer, Servomex 1410, should be turned on minimum 4 hours before use for the monitor to be stabilised. The air entering the system is compressed to 0.5 bar and the gas mixture flow should be adjusted to around 500 ml/min before it enters the gas analyser.

Besides zero calibrated with air, the gas analyser is also span calibrated with 5.0 vol. % propane (95% nitrogen) gas. The calibrated gas allowed to passing though the analyser at least 60 sec before the reading stabilised. The screws labelled SPAN 1 and SPAN 2 are used when adjustments for the calibrations needed. SPAN 1 is used when coarse adjustment is required while SPAN 2 is for fairly adjustment.

The analyser has an accuracy of ± 2% FSC.

It was recommended that the zero calibration should be checked weekly and both zero and span calibration checked monthly and adjust as necessary.

The measurement is based on the energy absorbed by the gas in the measuring cell at specific wavelength determined by the infrared filter. The degree of the absorption depends mainly on the number of absorbing molecules in the optical path and therefore on the pressure and the temperature of the sample.

Since the normal mode of operation is to discharge the sample from the cell at atmospheric pressure, the sensitivity of the analyser will be proportional to the atmospheric pressure. The effect is that of span change, so the error introduced is zero at zero concentration and maximum at full scale (i.e. analyser must obey the gas law effects). A change of 1% in the atmospheric pressure will cause a change of typically 1% of reading. The effect of changes in ambient temperature is less than 0.2 % FSD + 0.4 % of reading per °C.

When the gas concentration in the sample mixture is out of the limits the green alarm LED will switch off and a flashing red LED will come on. The alarm will be cancelled when the concentration returns to a safe level. The concentration alarm set point is adjusted by the rotary control on the front panel and by pressing the alarm set switch the alarm level will be indicated on the display.

For more information about the concentration alarm setting refers to chapter 3.4 in the instruction manual.

B.5 The discharge capacitors

In the present work, when working with ASTM, tailor made discharge capacitors of values in the range of 9-106 pF were used. As shown in Figure B.4, the capacitors consisted of two equally sizes epoxy FR4 plates of 1.5 mm thickness, and covered with a 35 µm layer of copper, connected to each other. The values of the capacitors were measured by using a handheld LCR meter, Smart Tweezers, which has an accuracy of 3%. The values of the capacitors are proportional with the area of the plates.

***Figure B.4**: The capacitors consisted of 2 equal sizes epoxy glass plates.*

B.5 Photos of the apparatuses

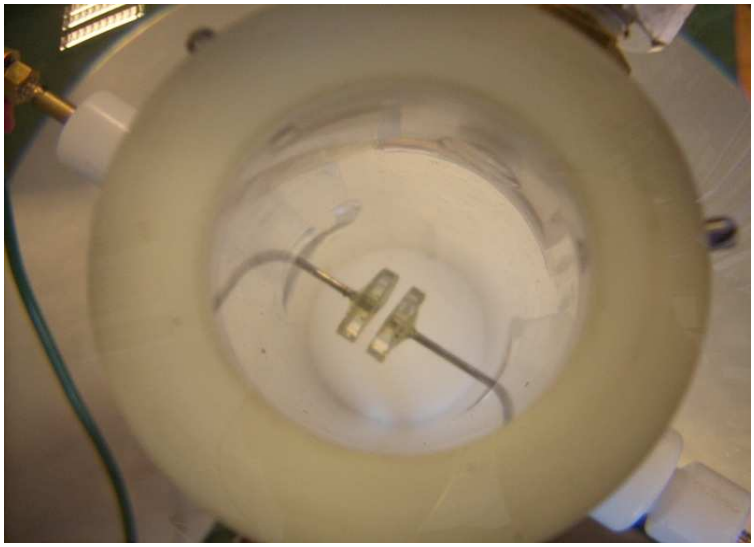

Figure B.5*: The glass flanged electrodes. The picture is taken from the top of the explosion vessel.*

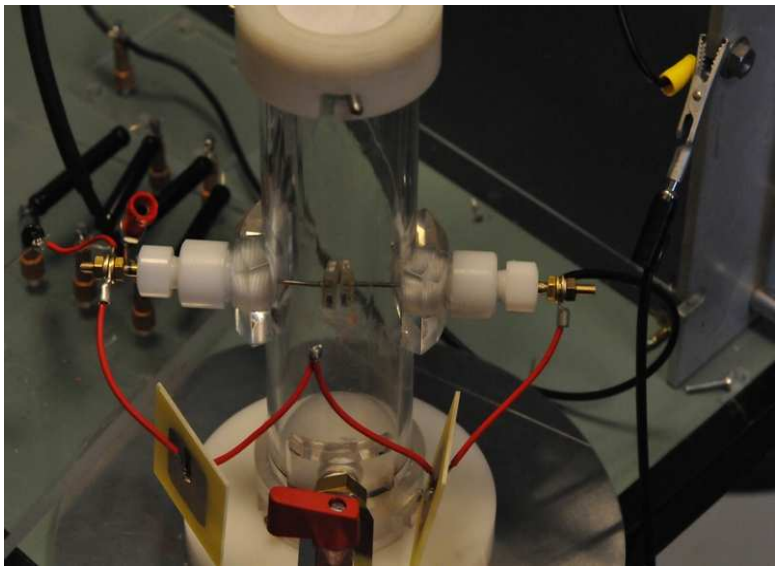

Figure B.6*: The explosion vessel connected to resistors in series of value of 10^{12} ohms. The capacitors consisted of two equal sizes epoxy glass FR4 plates are connected to the spark gap. A locking ring for fixing paper cover is placed at the top of the vessel.*

APPENDIX C: THE MODIFIED SYNCHRONIZED SPARK CIRCUIT.

C1. Circuit diagrams

Figure C.1 shows the circuit diagram of the pulse-generator P1 in Figure 3.5. When the pulse-generator is triggered, pulse A is generated. Pulse A has duration of 1.2 s. Pulse B has duration of 300 µs and is triggered by pulse A. The two output pulses from this pulse-generator are rectangular pulses of 60 µs duration each, 240 µs apart. These two pulses are used to trigger the pulse generator P2 and P3 in Figure 3.5.

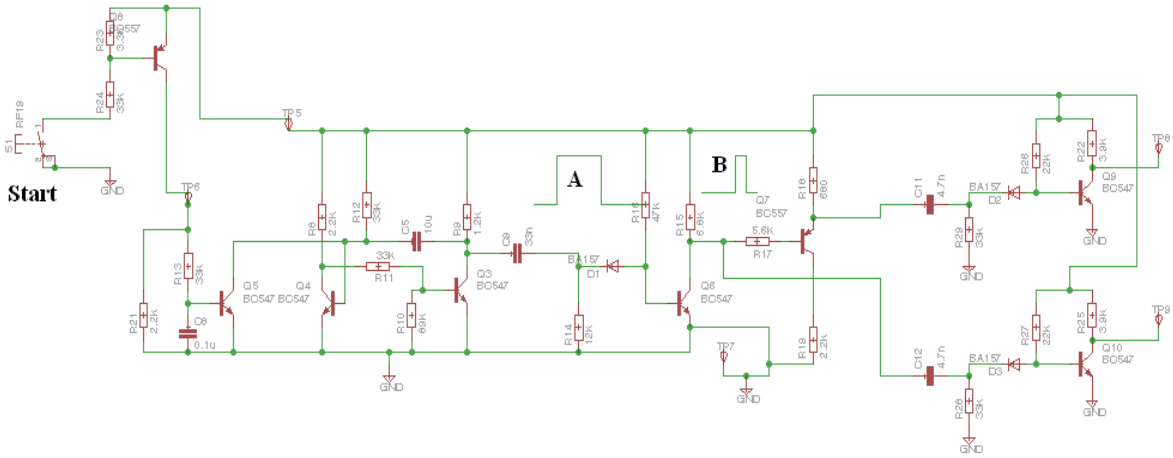

***Figure C.1**: Circuit diagram of pulse-generator P1.*

Figure C.2 shows the circuit diagram of amplifier A1 and the transformer T1 in Figure 3.5. This is standard current amplifier. The output pulse from this amplifier has shape and duration as shown in Figure 3.6a.

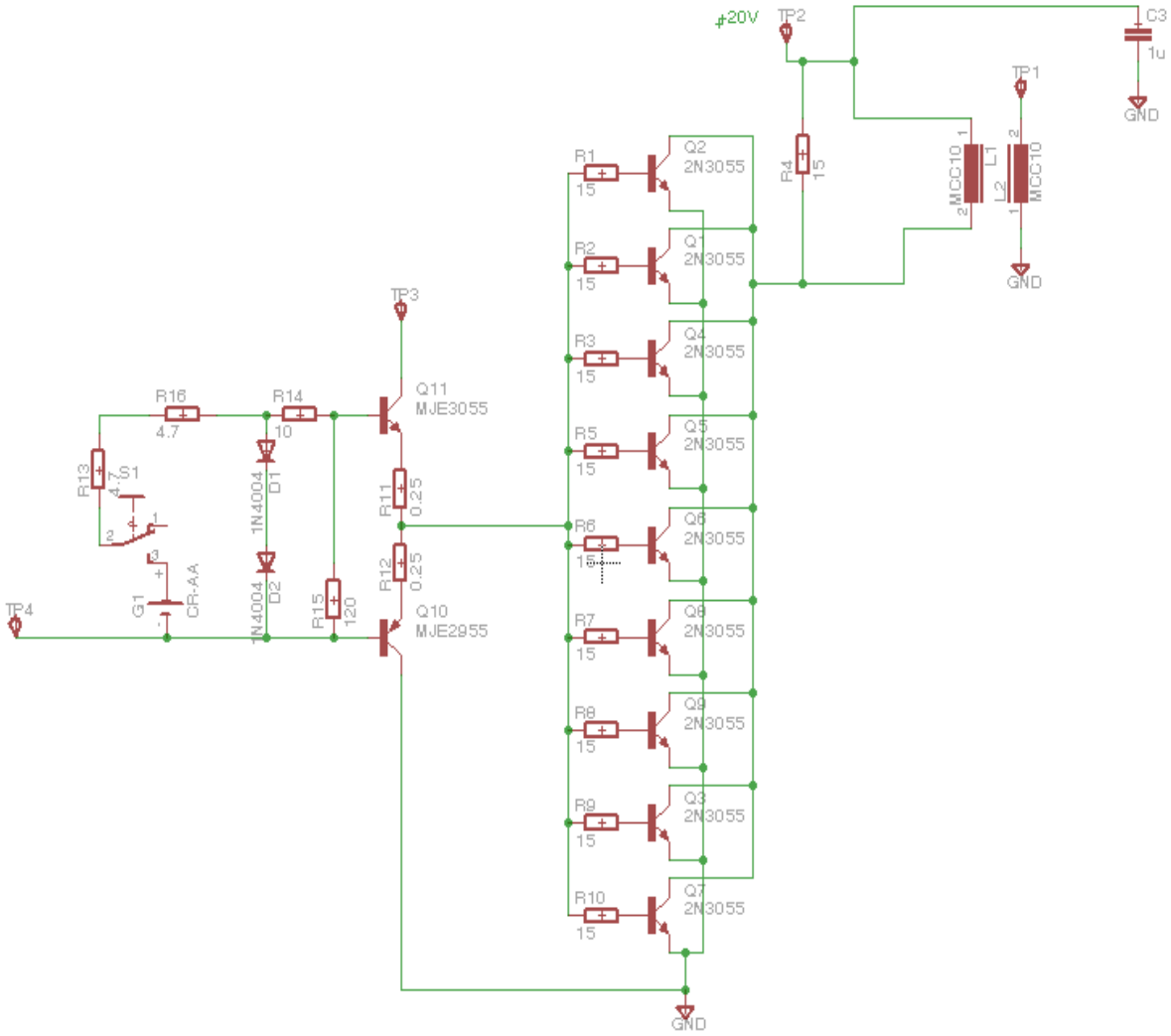

***Figure C.2**: Circuit diagram of amplifier A1.*

Figure C.3 shows the circuit diagram of amplifiers A2, A3 and the high-voltage transformer T2 in Figure 3.5. The two pulses from Figure 3.6b enter the amplifier A2 and A3, where they are amplified and combined to one pulse. The 6 NPN transistors are connected in parallel to amplify the current more effectively. With the aim to even the current, the resistors R5-R10 are inserted.

The high-voltage transformer T2 consists of two ferrite cores, with two windings on the primary side and 40 on the secondary side. With the aim to minimize the amplitude of the undershoot, the diode D2 is introduced.

The output pulse is a high-voltage pulse as shown in Figure 3.6e.

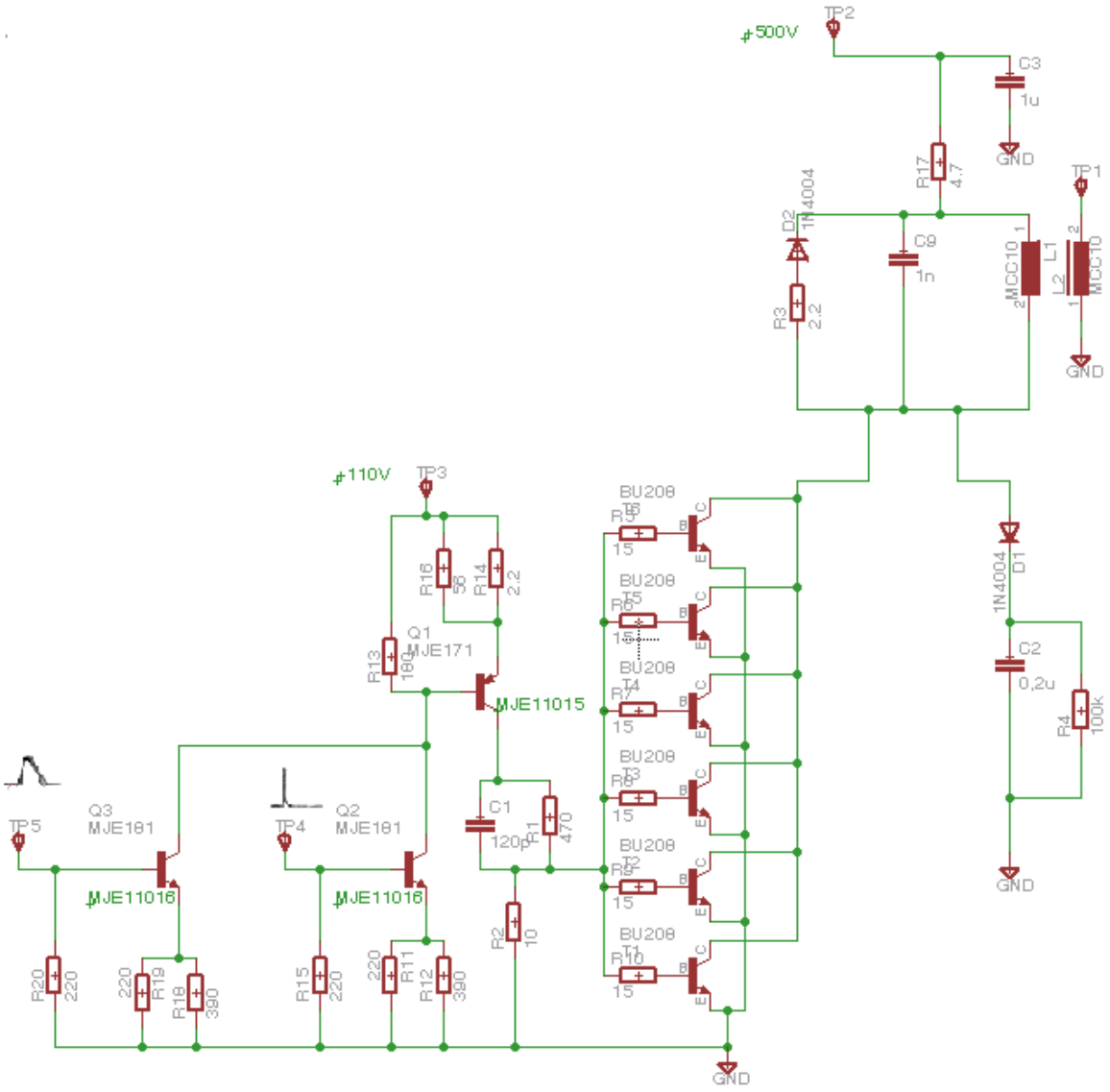

***Figure C.3**: Circuit diagram of amplifier A2,A3 and the high-voltage transformer T2.*

Figure C.4 shows the circuit diagram of the pulse filter F2 in Figure 3.5.
The capacitor C9, C12, C16 and C17 are inserted to minimize the noise influence. The function of R4, R15, R18 and the two transistors Q3-s is to amplify the current without changing the shape of the pulse. The diode D3 and D4 eliminate the 10 V peak pulse (after a downscale of 1000:1). The output pulse from F2 is an undershoot of around 0.1 V.

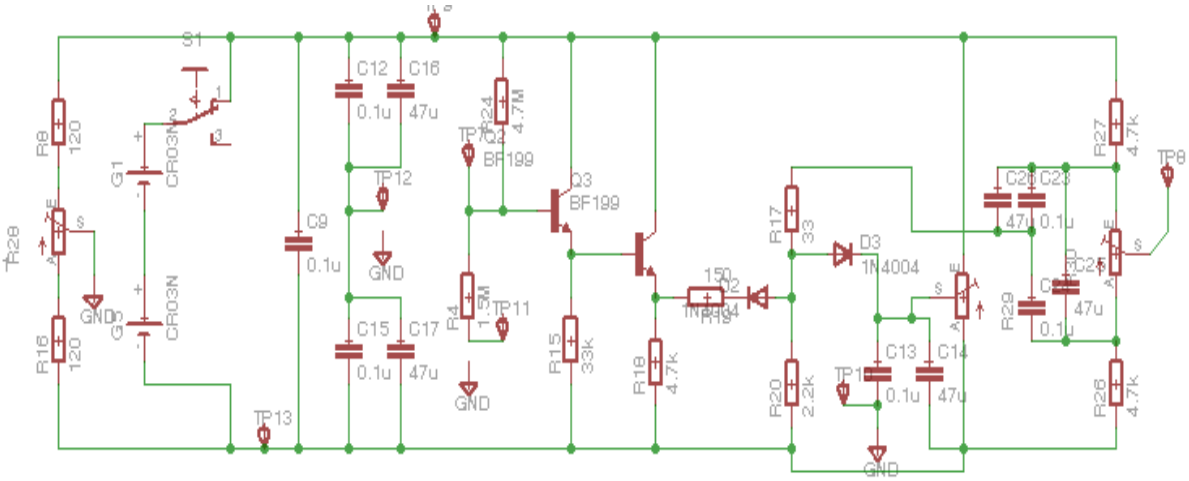

***Figure C.4**: Circuit diagram of the pulse filter F2.*

Figure C.5 shows the circuit diagram of the amplifier A4. This is a standard amplifier. The value of the connected capacitor C7 can be adjusted to achieve the desired pulse shape.

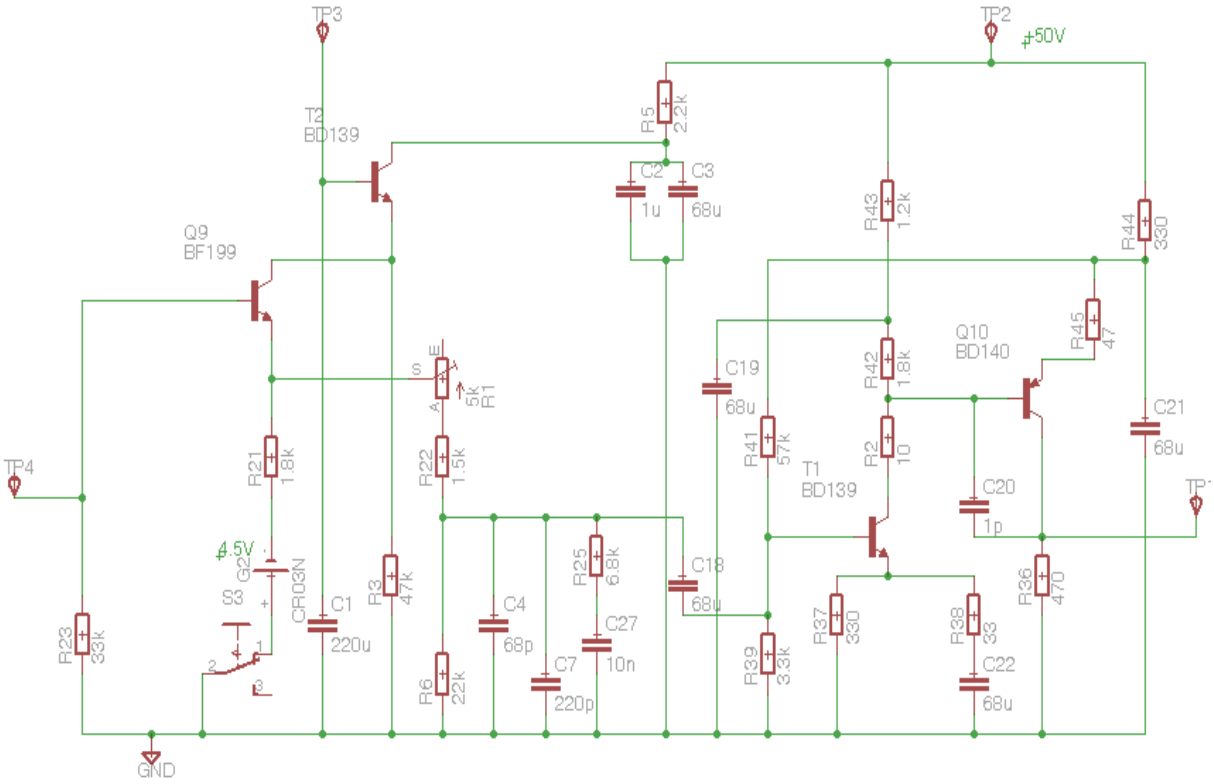

***Figure C.5**: Circuit diagram of the amplifier A4.*

Figure C.6 shows the circuit diagram of the amplifier A5. This is linear amplifier. The output pulse from A5 would have the same shape as the input pulse, only the voltage is amplified.

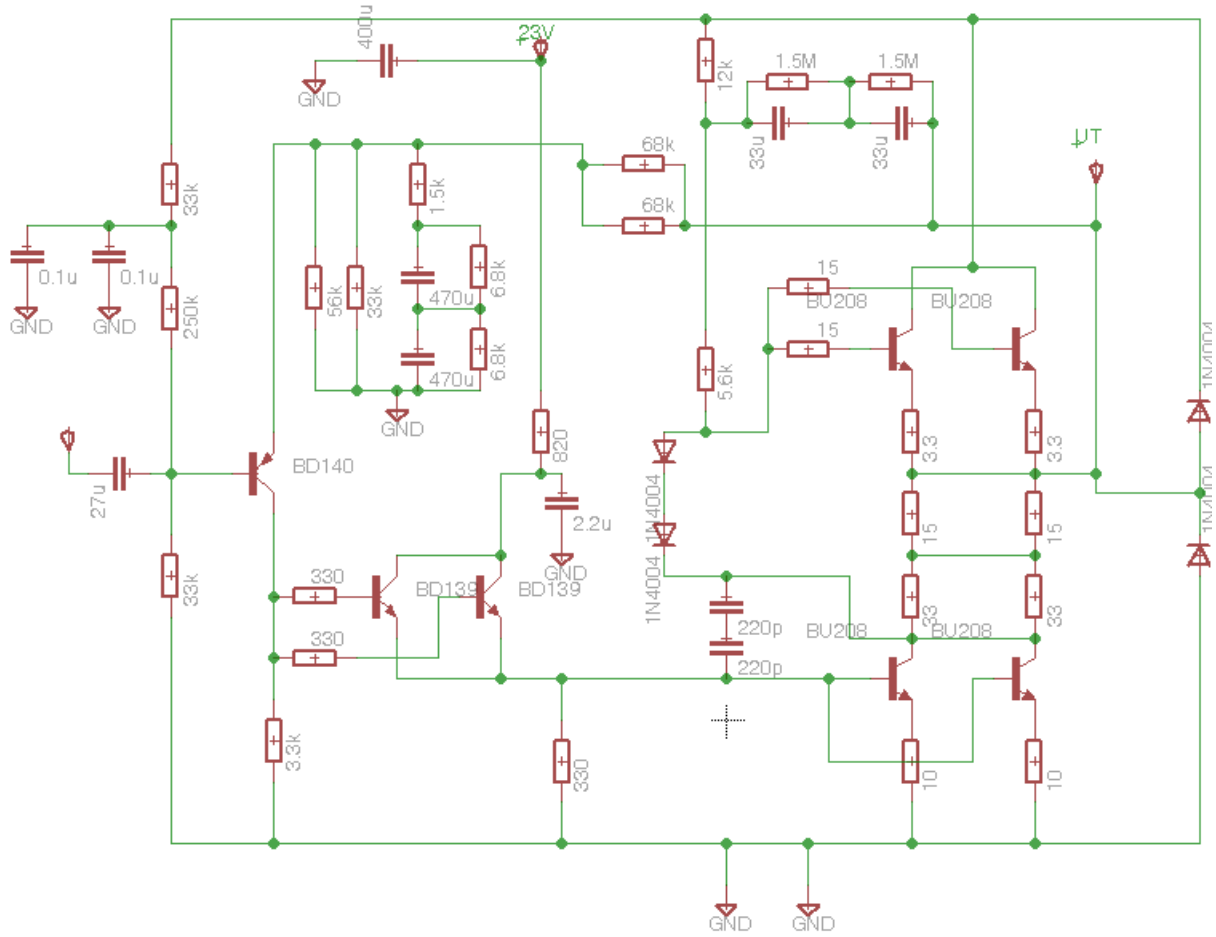

***Figure C.6**: Circuit diagram of amplifier A5.*

C2. Experimental results

C2.1 Summary of the test results obtained by using the new synchronized spark generator

Test nr.	V_0 (kV)	V_1 (kV)	C (pF)	R (kΩ)	Ignition / no-ignition (1/0)	E_1 (mJ)	E_2 (mJ)	E (mJ)
1	10.6	10.1	7.0	39	1	0.36	0.24	0.59
2	1.06	10.1	7.0		0	0.36	0.24	0.59
3	10.6	10.1	7.0		0	0.36	0.24	0.59
4	10.6	10.1	7.0		1	0.36	0.24	0.59
5	10.4	9.90	7.0		0	0.34	0.23	0.57
6	10.4	9.90	7.0		0	0.34	0.23	0.57
7	10.4	9.90	7.0		0	0.34	0.23	0.57
8	10.6	10.1	7.0		1	0.36	0.24	0.59
9	10.4	9.90	7.0		0	0.34	0.23	0.57
10	10.4	9.90	7.0		0	0.34	0.23	0.57
11	10.6	10.1	7.0		0	0.36	0.24	0.59
12	12.0	11.7	5.3		1	0.36	0.28	0.64
13	10.2	9.96	5.3		0	0.26	0.23	0.50
14	10.2	9.96	5.3		0	0.26	0.23	0.50
15	10.2	9.96	5.3		0	0.26	0.23	0.50
16	10.2	9.96	5.3		0	0.26	0.23	0.50
17	10.2	9.96	5.3		0	0.26	0.23	0.50
18	10.4	10.2	5.3		0	0.27	0.24	0.51
19	10.4	10.2	5.3		0	0.27	0.24	0.51
20	10.4	10.2	5.3		0	0.27	0.24	0.51
21	10.6	10.4	5.3		1	0.28	0.24	0.53
22	10.2	9.96	12.0		1	0.60	0.23	0.83
23	10.6	10.4	12.0		1	0.64	0.24	0.89
24	10.6	10.6	2.0		1	0.11	0.25	0.36
25	12.0	12.0	2.0		1	0.14	0.28	0.43
26	12.0	12.0	2.0		0	0.14	0.28	0.43
27	12.0	12.0	2.0		0	0.14	0.28	0.43
28	12.0	12.0	2.0		0	0.14	0.28	0.43
29	12.0	12.0	2.0		0	0.14	0.28	0.43
30	11.0	9.48	12.0		0	0.54	0.22	0.76
31	11.0	9.48	12.0		0	0.54	0.22	0.76
32	11.0	9.48	12.0		0	0.54	0.22	0.76
33	11.0	9.48	12.0		1	0.54	0.22	0.76
34	11.0	10.3	4.0	110	0	0.21	0.09	0.30

Test nr.	V_0 (kV)	V_1 (kV)	C (pF)	R (kΩ)	Ignition / no-ignition (1/0)	E_1 (mJ)	E_2 (mJ)	E (mJ)
35	11.0	10.3	4.0		0	0.21	0.09	0,30
36	10.8	10.1	4.0	110	0	0.20	0.08	0.29
37	10.0	9.35	4.0		0	0.17	0.08	0.25
38	11.2	10.5	4.0		0	0.22	0.09	0.31
39	11.0	10.3	4.0		0	0.21	0.09	0.30
40	1.10	10.3	4.0		0	0.21	0.09	0.30
41	10.0	9.35	4.0		0	0.17	0.08	0.25
42	11.0	10.3	4.0		0	0.21	0.09	0.30
43	10.0	7.65	7.0		0	0.20	0.06	0.27
44	9.80	7.49	7.0		0	0.20	0.06	0.26
45	10.4	7.95	7.0		0	0.22	0.06	0.29
46	12.0	12.0	2.0	165	0	0.14	0.10	0.24
47	12.0	12.0	2.0		0	0.14	0.10	0.24
48	12.0	12.0	2.0		0	0.14	0.10	0.24
49	11.8	11.8	2.0		0	0.14	0.10	0.24
50	11.2	11.2	2.0		0	0.13	0.09	0.22

C2.2 Photos of pulse signals produced by the new synchronized spark generator

The yellow pulse is recorded by placing the high-voltage probe in prior to the spark as shown in Figure 3.5. The green and blue pulse are the undershoot of the yellow pulse, recorded from the same place, on the other side of the spark gap.

Figure C6-C9 shows the shape and size of undershoot of the pulse vary from test to test, indicating the new spark generator requires further improvements.

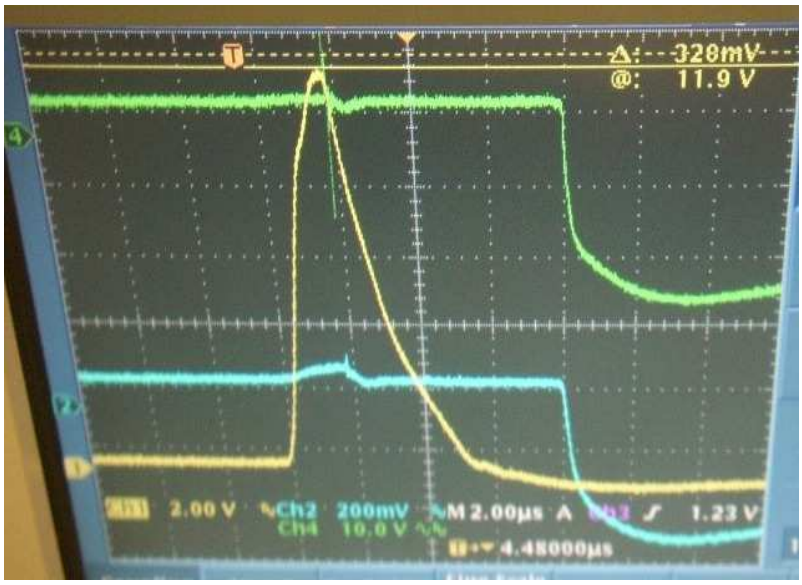

***Figure C.6**: Pulses over the spark gap at spark discharge.*

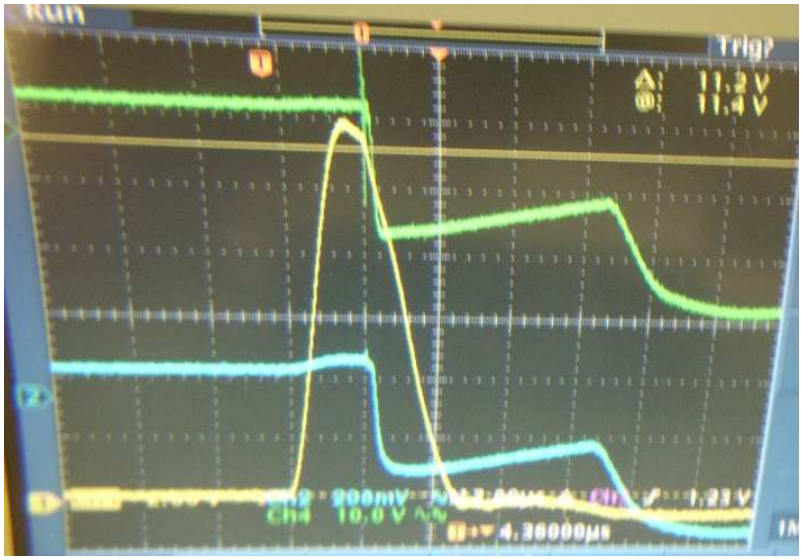

***Figure C.7**: Pulses from both side of spark gap at spark discharge.*

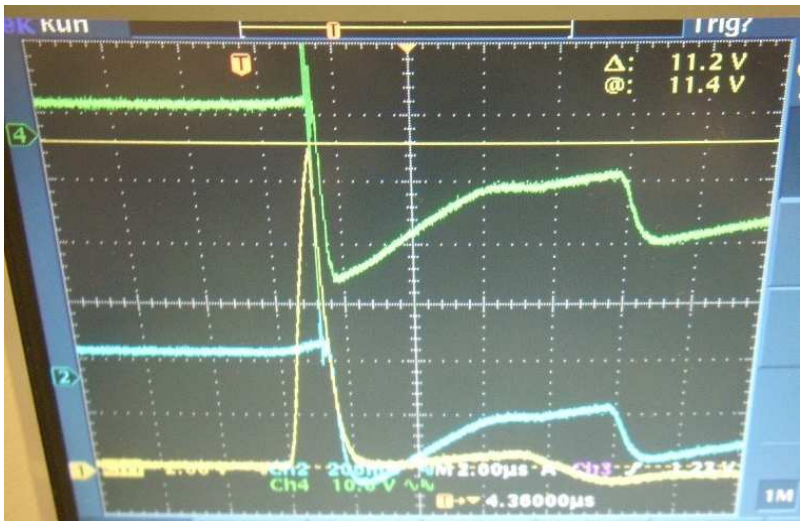

***Figure C.8**: Pulses from both side of spark gap at spark discharge.*

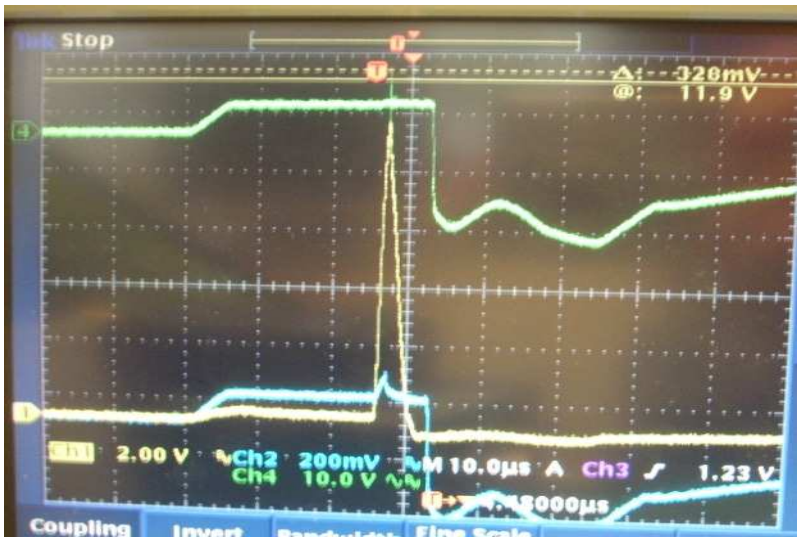

***Figure C.9**: Pulses from both side of the spark gap at spark discharge.*